J. Fluid Mech. (1989), *vol.* 203, *pp.* 347–380
Printed in Great Britain

The generation and collapse of a foam layer at the roof of a basaltic magma chamber

By CLAUDE JAUPART AND SYLVIE VERGNIOLLE
Laboratoire de Dynamique des Systèmes Géologiques, Université Paris 7 et Institut de Physique du Globe, 4 place Jussieu, 75252 Paris, Cedex 05, France

(Received 21 July 1988)

Basaltic volcanoes erupt in several different regimes which have not been explained. At Kilauea (Hawaii), eruption can take the form of either fire fountaining, where gas-rich jets propel lava clots to great heights in the atmosphere, or quiet effusive outflow of vesicular lava. Another regime is commonly observed at Stromboli, where large gas slugs burst intermittently at the vent. In an attempt to provide a unifying framework for these regimes, we investigate phenomena induced by degassing in a reservoir which empties into a small conduit. Laboratory experiments are done in a cylindrical tank topped by a thin vertical tube. Working liquids are silicone oils and glycerol solutions to investigate a range of viscosity and surface tension. Gas bubbles are generated at the tank bottom with known bubble diameter and total gas flux. The bubbles rise through the tank and accumulate in a foam layer at the roof. Depending on the behaviour of this foam layer, three different regimes can be distinguished: (i) steady horizontal flow of the foam leading to bubbly flow in the conduit; (ii) alternating regimes of foam build-up and collapse leading to the eruption of a single, large gas pocket; (iii) flow of the foam partially coalesced into larger gas pockets leading to intermittent slug flow in the conduit. These regimes have natural counterparts in basaltic volcanoes.

A simple theory is proposed to explain regimes (i) and (ii). The bubbles in contact with the roof deform under the action of buoyancy forces, developing flat contact areas whose size increases as a function of foam thickness. Maximum deformation corresponds to a critical thickness $h_c = 2\sigma/\epsilon\rho_l gR$, where σ is the coefficient of surface tension, ρ_l the liquid density, g the acceleration due to gravity, R the bubble radius and ϵ the gas volume fraction in the foam. The foam thickness is determined by a balance between the input of bubbles from below and the output into the conduit, and is proportional to $(\mu_l Q/\epsilon^2\rho_l g)^{\frac{1}{4}}$, where μ_l is the liquid viscosity and Q the gas flux. A necessary and sufficient condition for collapse is that it exceeds the critical value h_c. In a liquid of given physical properties, this occurs when the gas flux exceeds a critical value which depends on viscosity, surface tension and bubble size. Experimental determinations of the critical gas flux and of the time between two events of foam collapse are in agreement with this simple theory.

1. Introduction

Our understanding of volcanoes has progressed in recent times thanks to detailed and continous monitoring of volcanic activity in several permanent observatories throughout the world, and to a large number of geophysical and geochemical investigations. The structure of the volcanic edifice, the plumbing system used by lava to reach the Earth's surface, and the evolution of lava composition are well

documented for several volcanoes. The dynamics of eruptive phenomena has, however, received less attention. Part of the reason for this lies in the high complexity of volcanic flows, which involve suspended crystals and gas bubbles. The main reason is perhaps that it is difficult to relate eruptive phenomena to specific processes occurring at depth, either in the superficial magma chamber or in the deeper source of molten material.

To set the scene for the present paper, we describe three basic eruption regimes representative of basaltic volcanoes. At Kilauea volcano (Hawaii), eruption can take the form of 'fire fountaining', where lava clots are propelled to heights of several hundred metres in the atmosphere by a powerful gas-rich jet (Swanson *et al.* 1979). Another possible regime at Kilauea is the effusive one, where vesicular lava oozes out of the vent. At Stromboli, eruptive activity often takes the form of intermittent explosions due to the bursting of large gas pockets which are almost as wide as the volcanic conduit (Blackburn, Wilson & Sparks 1976; Wilson 1980). There is at present no unifying theory to explain these different regimes.

We focus on Hawaiian eruptions because we believe they provide a unique opportunity to probe into the magma chamber itself. The striking feature of these eruptions is continuous 'fire fountaining' which lasts for several hours (up to twenty in the last Pu'u'Oo eruption of 1983–1986). This magnificent type of activity represents only a small fraction of the whole eruptive sequence. Consider for example the 1969–1971 Mauna Ulu eruption (Swanson *et al.* 1979). During the first six months, twelve episodes of fire fountaining were interspersed with long episodes of quiet effusive activity lasting several weeks. For the next eighteen months, the eruption continued without fire fountaining, in an effusive regime which slowly waned. This reveals two important features: first, cyclic changes of activity in the first part of the eruption, secondly, the disappearance of fire fountaining in the second part. These same features have been recorded for other Hawaiian eruptions and are thus truly representative.

It is instructive to compare the duration of each phase in the cyclic regime with the rise-time from chamber to vent. At Kilauea, the top of the main magma chamber is at a depth of 2–3 km (Thurber 1987; Ryan 1987). Eruptions occur either at the summit of the volcano, or many kilometres away on its east flank, about 10 km in the Mauna-Ulu case discussed here. The horizontal extent of the chamber is not known accurately and it is not clear how far it extends in the direction of the flank eruptive vents. Thus, the distance from the chamber to the vent is only constrained to be between about 3 and 10 km. During fire fountaining, lava clots and gas are erupted at velocities of several hundred metres per second (Wilson & Head 1981). These high velocities are due to gas exsolution and expansion as pressure is released during ascent in the conduit. Taking into account the pressure effect leads to a representative value of 1 m/s for velocities at depth, regardless of the exact flow regime (Wilson & Head 1981; Vergniolle & Jaupart 1986). Thus, an upper bound for the rise-time from chamber to vent is 3 h, which is less than 10 h, the typical duration of a fountaining episode. Because the characteristics of fire fountaining remain quasi-steady throughout an episode, this implies that conditions at the conduit entrance, i.e. at the chamber roof, are also steady during this length of time. The same conclusion holds for effusive activity. Flow velocities are around 10^{-2} m/s (Vergniolle & Jaupart 1986) and the rise-time cannot exceed 12 days, which is again significantly lower than the episode duration (typically a month). We conclude that both regimes are close to steady-state and hence that they correspond to different conditions in the

reservoir which feeds the conduit. Cyclic activity thus reflects cyclic changes in the magma chamber.

The quantity of volatile species which can be dissolved in silicate magmas increases with increasing confining pressure. All magmas generated in the earth contain sufficient volatiles such that, during decompression on their ascent to the surface, exsolution of gas bubbles occurs. A central issue is whether or not bubbles are present in shallow magma chambers beneath volcanoes or whether they first appear during the final ascent through the eruption conduit. Available physical models (e.g. Wilson & Head 1981) deal with the evolution of a homogeneous mixture of magma and gas as it rises in the eruption conduit and undergoes pressure release. In steady-state conditions, these models are able to predict the eruption characteristics as a function of mass flux and lava volatile content. However, they rely on simplifying assumptions on the pressure evolution and the interaction between the liquid and gas phases (Vergniolle & Jaupart 1986). As a consequence, they are weakly sensitive to conditions in the chamber that feeds the eruption. When the eruption characteristics vary, these models are used to infer that the gas content of lava changes (Head & Wilson 1987), but the cause of these changes is not explained. Our aim is to propose a model based on separated flow of gas and liquid in the magma chamber and conduit system. This model links observed eruptive characteristics, including intermittent changes of regime, to processes occurring in the magma chamber and/or specific locations in the plumbing system of the volcano.

Several pieces of evidence provide a clue as to the mechanism which is at work. At Stromboli, detailed measurement of exit velocities show that the volume ratio of gas to lava is very large, typically about 10^5 (Chouet, Hamisevicz & McGetchin 1974). Such extreme values cannot be explained by gas exsolution and expansion during ascent in the conduit, and thus imply that volatile concentration is occurring at depth. At Etna, the compositions of gases and lava in radioisotopes with short half-lives imply that lava remains in contact with a gas phase for several days before being erupted (Lambert *et al.* 1985; LeCloarec *et al.* 1988). These studies indicate that magma and gas phases coexist in a deep reservoir throughout an eruption. A similar conclusion is reached for Kilauea on the basis of the carbon–sulphur systematics of erupted gases (Greenland 1987). One reason why gas exsolution can begin in the magma chamber is because the melt is stored there; it loses heat to the surrounding solid rocks which in turn causes crystallization. Volatile species are essentially incompatible in the mineral phases and hence fractional crystallization concentrates volatiles in the melt until the saturation point is reached (Tait, Jaupart & Vergniolle 1989).

Motivated by the evidence that a gas phase is present in the magma chamber, we have studied in the laboratory the dynamical phenomena induced by degassing in a reservoir which empties into a narrow conduit (Jaupart & Vergniolle 1988). Specifically, degassing takes the form of gas bubbles, which rise through liquid and are trapped at the reservoir roof, where they accumulate in a foam layer. This foam collapses periodically into gas pockets which erupt into the conduit. The purpose of the present study is to present a complete set of experimental results, including measurements of intermittency and erupted gas volumes, together with a simple theory to account for them. The limitations and implications of the model are discussed in the last section.

2. The experiments

2.1. *Experimental set-up and working fluids*

Our apparatus is described in figure 1. A cylindrical tank of 14 cm inner radius is topped by a conduit of 2.2 cm inner radius. Gas bubbles are generated at the bottom through a set of 185 capillary tubes connected to a pressurized nitrogen bottle. The gas flux is monitored. The capillary tubes all have the same width and length, ensuring that the viscous head loss is constant and hence that the emitted bubbles have the same size. To verify that the phenomena observed were not an artefact of the apparatus, we also used a larger conduit (5 cm radius) and a smaller number (45) of capillary tubes.

We use silicone oils with viscosities ranging from 10^{-2} to 5 Pa s (table 1). To investigate the role of surface tension, we also used glycerol solutions of various concentrations. These have the same viscosity values as some of the silicone oils but have surface tension coefficients which are higher by a factor of 3.

Depending on the gas flux, there are two regimes for bubble generation out of capillary tubes (Clift, Grace & Weber 1978, pp. 324–327). At low gas flux, the bubble diameter is determined by the balance between buoyancy and surface tension around the orifice perimeter:

$$d = \left(\frac{6 d_0 \sigma}{\rho_1 g}\right)^{\frac{1}{3}}, \tag{1a}$$

where d_0 is the orifice diameter, σ the surface tension coefficient, ρ_1 the liquid density, and g the acceleration due to gravity. At higher gas flux, the bubble diameter is determined by a balance between buoyancy and drag by flow. Denoting the gas flux by Q and the number of capillary tubes by n, the gas flux for each orifice is Q/n and the bubble diameter is given approximately by:

$$d = 2.3\left(\frac{\mu_1 Q}{n \rho_1 g}\right)^{\frac{1}{4}}, \tag{1b}$$

where μ_1 is the liquid viscosity. We have verified the validity of these formulae by using photographs taken from the top of the open tank. The bubble diameters are given in table 2 as a function of working fluid and gas flux for the set of 185 capillary tubes.

2.2. *The different regimes observed*

The experiments have been described earlier (Jaupart & Vergniolle 1988), and we briefly recall the salient results. As the gas flux is increased, the bubbles rise in increasingly complex patterns, eventually forming bubble plumes. The patterns also depend on liquid viscosity. They are due neither to the roof and conduit geometry, as shown by experiments with the tank open, nor to the capillary tube arrangement, as shown by experiments in water where each bubble rises perfectly vertically. For our present purposes, these phenomena play no important role and it may be assumed that there is a uniform supply of bubbles at the tank roof.

For any given liquid, the experiment can be characterized by the dynamic phenomena which occur but, more importantly, by the level of liquid in the conduit. As gas is fed into the tank, liquid rises in the conduit to compensate for the gas volume contained in the tank. This gas volume is the sum of two contributions, one

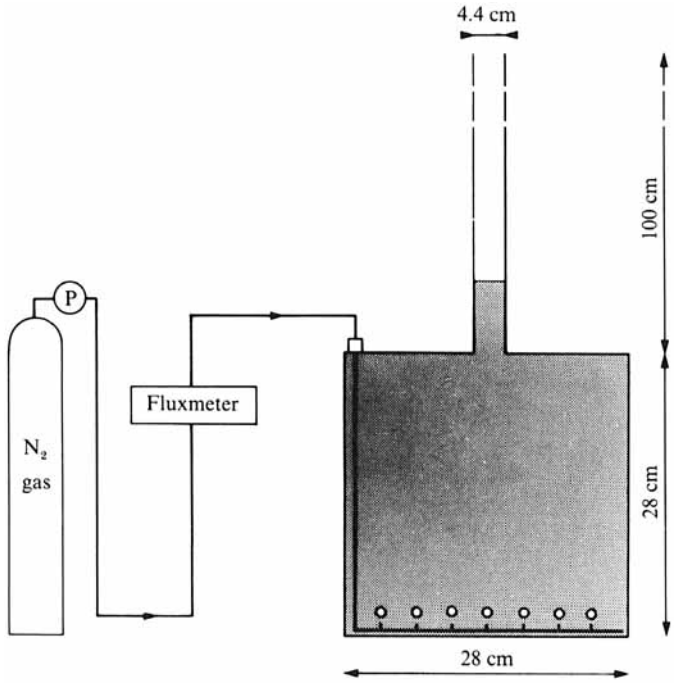

FIGURE 1. Experimental set-up to study the phenomena induced by degassing in a reservoir. Gas is injected through a set of 185 capillary tubes at the bottom of the tank. The gas flux is monitored through a fluxmeter.

	Density ρ_l (kg m^{-3})	Viscosity (at 21 °C) μ_l(Pa s)	Surface tension $\sigma(kg\ s^{-2})$
Silicone oils (Rhodorsil)			
47V10	930	9.3×10^{-3}	2.0×10^{-2}
47V50	950	4.8×10^{-2}	2.1×10^{-2}
47V100	965	9.7×10^{-2}	2.1×10^{-2}
47V500	970	4.9×10^{-1}	2.1×10^{-2}
47V1000	970	9.7×10^{-1}	2.1×10^{-2}
47V5000	973	4.9	2.1×10^{-2}
Glycerols			
85%	1228	1.5×10^{-1}	6.4×10^{-2}
87%	1237	2.0×10^{-1}	6.4×10^{-2}
99%	1262	1.2	6.3×10^{-2}

TABLE 1. Physical properties of the working liquids

from the bubbles rising in the tank and the other from the foam layer at the roof (figure 2). For a given gas flux, the former is constant and hence the 'activity' can be monitored by watching the variations of liquid level in the conduit. This simple observation has also been made on true volcanoes. We have characterized three different regimes. For the sake of simplicity, we describe them using the silicone oils

Gas flux (cm^3/min)	200	2000
Silicone oils		
47V10	1.7	1.7
47V50	1.7	2.3
47V100	1.7	2.7
47V500	2.3	4.0
47V1000	2.7	4.8
47V5000	4.0	7.6
Glycerols		
85%	2.3	2.8
89%	2.3	3.0
99%	2.7	4.7

TABLE 2. Bubble diameters (in mm)

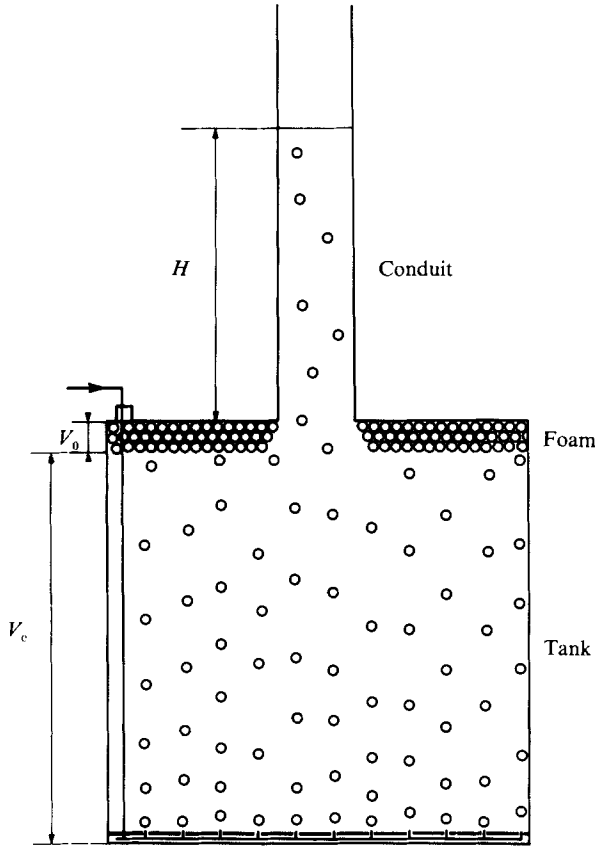

FIGURE 2. The liquid level in the conduit rises because of the gas contained in the system. This has two contributions: bubbles rising in the tank and bubbles included in the foam at the tank roof.

at a given gas flux of 1000 cm^3/min, as a function of liquid viscosity only. The role of the other parameters will be discussed later.

For the silicone oil with lowest viscosity (10^{-2} Pa s), the system reaches a steady state in which the foam flows horizontally along the tank roof and escapes into the conduit. The level of liquid in the conduit stays constant, which shows that the foam volume also stays constant.

For a viscosity five times higher (0.05 Pa s), the foam goes through a cycle of accumulation and collapse, reflected in large variations of liquid level in the conduit. As new gas bubbles reach the tank roof, the foam thickness increases and liquid rises in the conduit. When the foam reaches a certain thickness, it collapses suddenly into a single gas pocket which erupts (figure 3). As the volume of gas trapped in the foam is lost, the liquid level drops in the conduit.

For liquid viscosity exceeding 0.5 Pa s, the foam collapses only partially and generates a series of gas slugs which erupt intermittently (figure 4). The level of liquid in the conduit exhibits small fluctuations associated with the bursting of these slugs.

The experiments thus show three different regimes: (i) steady foam flow, (ii) alternating regimes of foam build-up and collapse leading to the violent eruption of a large gas pocket and (iii) partial foam collapse leading to intermittent slug flow. These regimes represent different states for the foam layer and define convenient limit-cases. The first regime is such that there is a permanent foam layer made of the bubbles fed through the tank bottom. In the second regime, there is no permanent foam layer and the system alternates between a state of foam build-up and one of foam disappearance. In the third regime, there is again a permanent foam layer at the tank roof, but it is made of gas pockets which are larger than the bubbles from the tank interior.

These regimes also depends on the gas flux and the coefficient of surface tension. To illustrate this, we have recorded the height of the liquid column in the conduit as a function of the gas flux. For each gas flux, we made a series of at least thirty such determinations and calculated the mean and the standard deviation. These data are converted to volume values using the conduit cross-section. As shown later, these straightforward and simple measurements are sufficient to characterize the processes occurring in the system in a quantitative manner.

Figure 5(*a*) shows the data for the liquid with lowest viscosity (10^{-2} Pa s). At any given gas flux, the liquid level is constant and hence takes a single value. This level rises as the gas flux increases because the volume of foam and the amount of bubbles in the tank both increase. The increase of foam volume will be explained in §3. The volume occupied by the rising bubbles is equal to the product of the gas flux and the rise-time from bottom to top. The bubble diameter is weakly sensitive to the gas flux (equations (1*a*, *b*)), implying that the rise velocity and hence the rise time depend weakly on the gas flux. Thus, increasing the gas flux leads to a larger number of gas bubbles in the tank interior. The foam volume is not absolutely constant, due to the fact that, as the foam flows against the roof, a few bubbles sometimes coalesce at the conduit edge and form a gas slug which rises and bursts at the top of the liquid column. The relevance of this phenomenon to what has been called 'gas piston' activity at Kilauea volcano has been discussed in Jaupart & Vergniolle (1988).

Figure 5(*b*) shows the data for the 0.05 Pa s silicone oil. We have already mentioned that this experiment is characterized by cyclic changes of liquid level due to foam collapse. In fact, it is only above a certain critical value of the gas flux that cyclic activity occurs. At low gas flux, the regime of steady foam flow prevails. Consider the minimum and maximum values of the gas volume contained in the tank

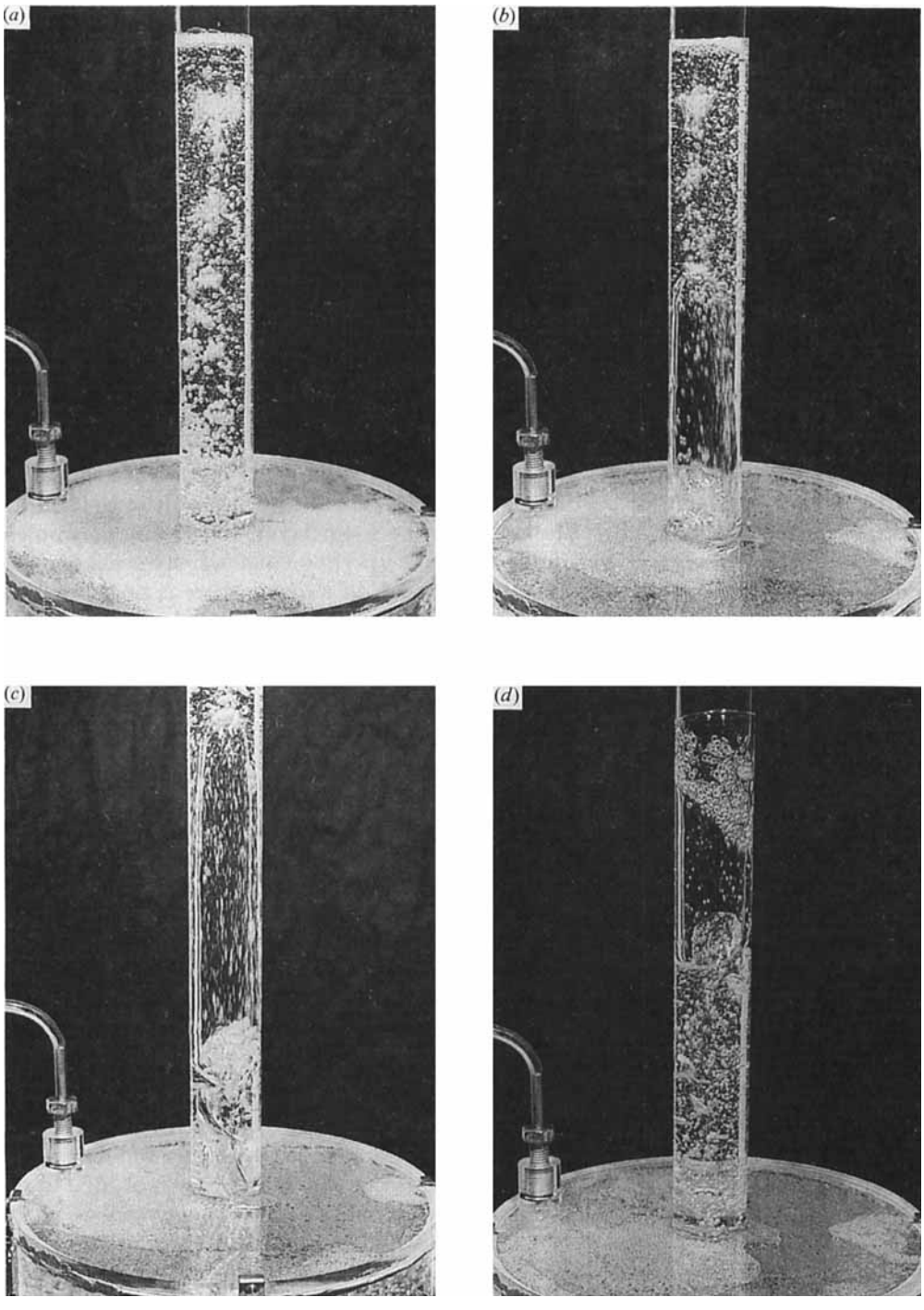

FIGURE 3. The alternating regimes of foam build-up and collapse for 0.1 Pa s silicone oil (the gas flux is 1000 cm^3/min). The photographs are taken at 0.5 s intervals. (*a*) The bubbles accumulate at the roof (white region) and liquid rises in the conduit. (*b*) At a critical thickness, the foam collapses into a single gas pocket which starts erupting. (*c*) The gas pocket erupts in an annular flow configuration, with a central gas jet and liquid films along the conduit walls. (*d*) The gas pocket has erupted: note the liquid projections at the conduit walls and the drop in liquid level.

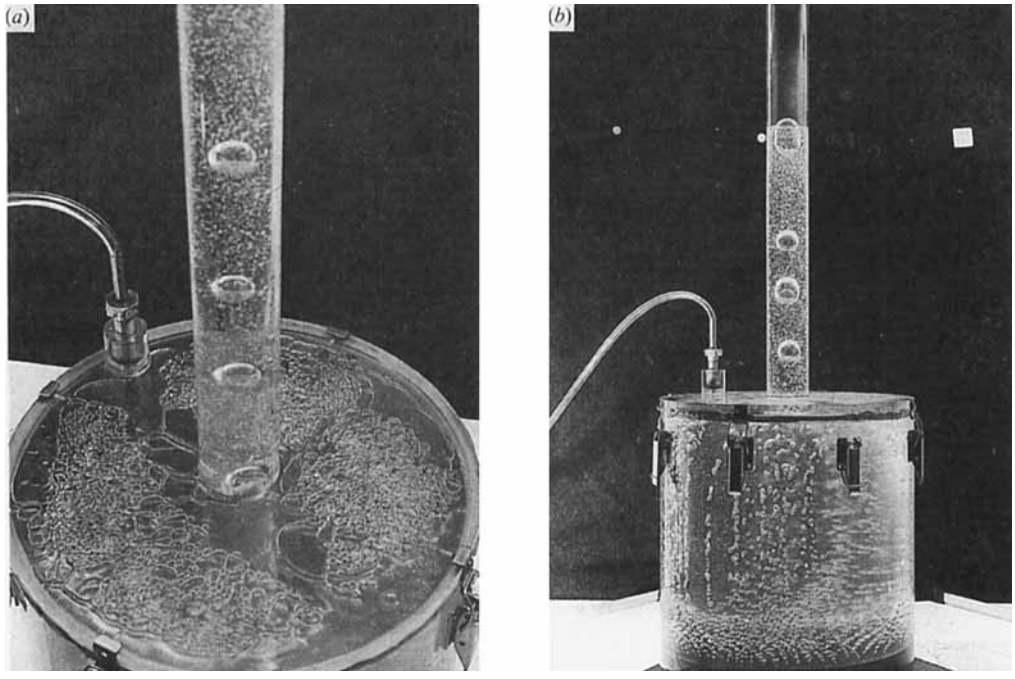

FIGURE 4. The intermittent slugging regime for 1 Pa s silicone oil. (*a*) Close-up of the tank roof showing that the foam is made of coalesced bubbles which erupt as gas slugs. (*b*) Gas slugs rising in the conduit. Note that they are much larger than the bubbles in the tank.

(figure 5*b*). These two values cannot be distinguished at low gas flux, which corresponds to the regime of steady foam flow. As the gas flux is increased, the curves for the minima and maxima diverge markedly, which marks the transition to the cyclic regime. The standard deviation of the measurements is not the same for both volumes. That for the maximum is markedly smaller than the other and is accounted for solely by the random coalescence events occurring at the conduit edge just described. This indicates that there is a well-defined maximum for a stable foam volume at the tank roof. In contrast, the minimum gas volume exhibits larger fluctuations because the gas pocket does not always erupt in a single piece. At a given gas flux, the difference between the two volumes gives the volume of the gas pocket which erupts. As shown by figure 5(*b*), this volume increases together with the gas flux.

To illustrate the role of surface tension, we compare in figure 5(*c*) the data for the 0.01 Pa s silicone oil and an 85% glycerol solution which has an almost identical viscosity (table 1). The onset of foam collapse occurs at a much higher gas flux in the case of the glycerol solution.

These data provide the framework for the model developed below. We have also recorded the time between 'bursts'. This second data set provides an independent check on the theory.

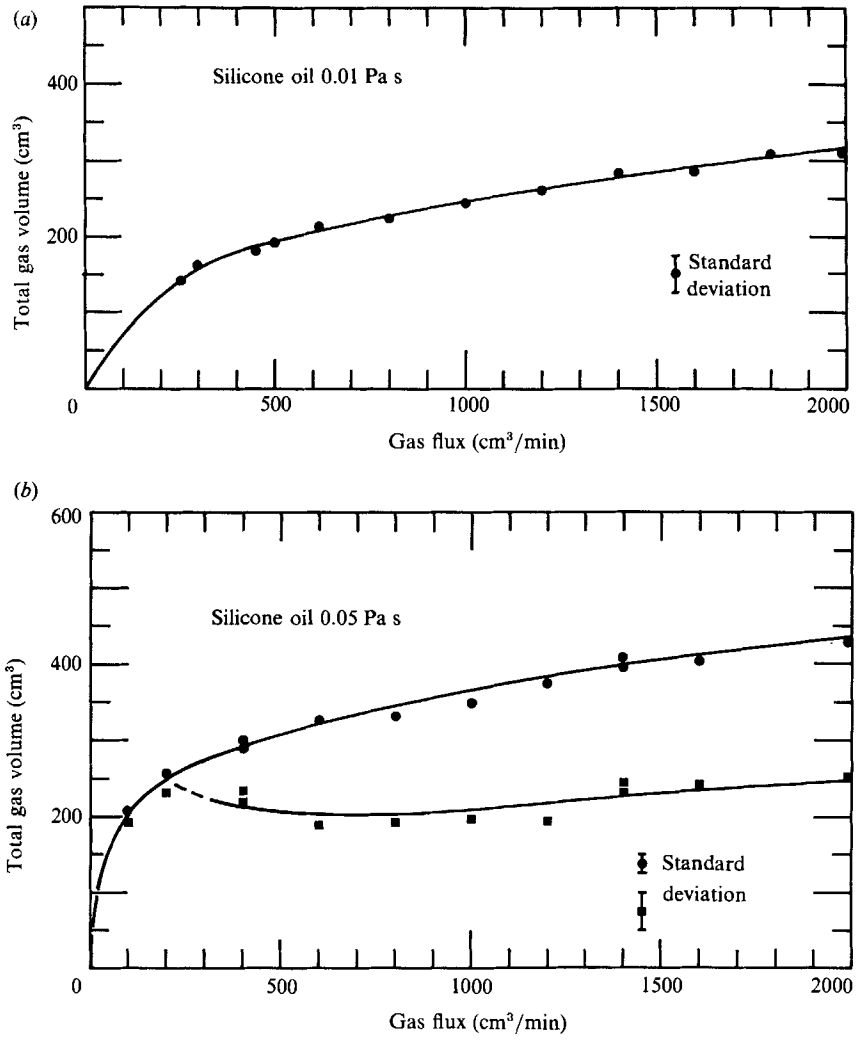

FIGURE 5(*a*, *b*). For caption see facing page.

3. Theoretical aspects

We proceed by a series of independent considerations which are discussed with the relevant observations.

3.1. *The flow of the foam layer at the tank roof*

The foam which accumulates at the tank roof flows towards the conduit and we treat it as a homogeneous fluid of effective density ρ_m and viscosity μ_m. The foam density is given by:

$$\rho_m = (1-\epsilon)\rho_l + \epsilon\rho_g, \tag{2a}$$

where ϵ is the volume fraction of bubbles within the foam and ρ_l and ρ_g the densities of liquid and gas respectively. Because the gas density is much less than that of liquid, a useful simplification is:

$$\rho_m = (1-\epsilon)\rho_l. \tag{2b}$$

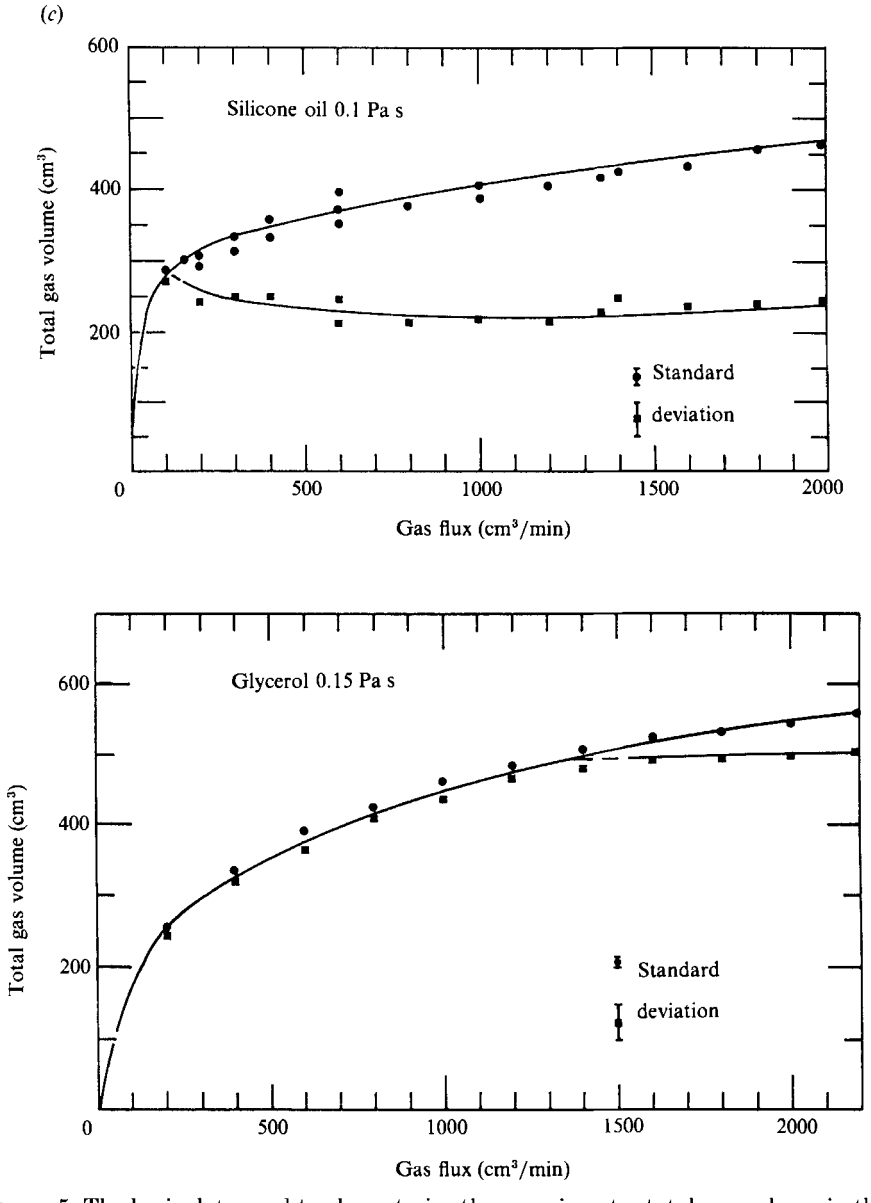

FIGURE 5. The basic data used to characterize the experiments: total gas volume in the system as a function of gas flux. (*a*) 0.01 Pa s silicone oil, the foam volume is constant at a given gas flux, which corresponds to steady foam flow towards the conduit. At the highest gas flux of 2000 cm³/min, the standard deviation is observed to increase and foam collapse is observed at about 2200 cm³/min. (*b*) 0.05 Pa s silicone oil. At values of the gas flux greater than about 200 cm³/min, the gas volume exhibits large fluctuations due to foam collapse. Two values of the gas volume are found for each gas flux: the smallest is equal to the volume of gas bubbles in the tank, the largest to that same volume plus the gas volume contained in the foam layer. The difference between the two is the volume of the gas pocket which erupts. (*c*) Comparison between a silicone oil and glycerol solution of similar viscosities. Note that it takes a larger gas flux to achieve foam collapse in the glycerol solution.

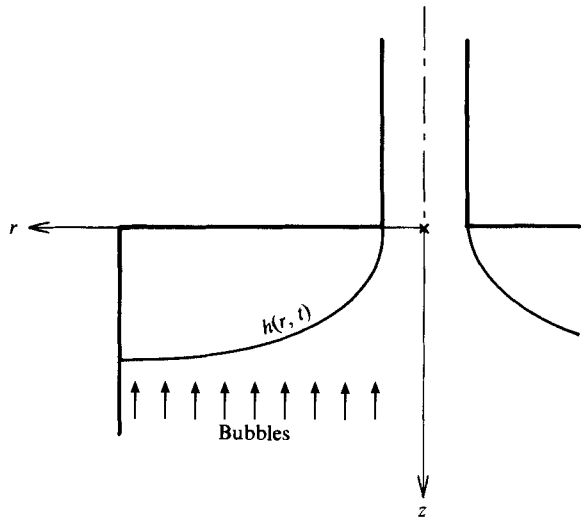

FIGURE 6. Coordinate system used to write down the equations for the flow of foam at the tank roof.

The flow properties of foams are not well known in the general case (Kraynick 1988). As discussed in Appendix A, a model appropriate for our experimental conditions is that of a Newtonian fluid with viscosity given by:

$$\mu_m = \mu_l(1-\epsilon)^{-\frac{5}{2}}. \tag{3}$$

This expression shows that foams are significantly more viscous than their parent liquid. The foam layers observed in our experiments are always thin, with horizontal dimensions far exceeding their height, and we use the lubrication approximation (Batchelor 1967, p. 219). They behave like viscous currents which are continuously fed from below by the bubbles rising from the tank interior (figure 6). In cylindrical coordinates (r, z), the equations of motion can be reduced to:

$$0 = -\frac{\partial P}{\partial z} + \rho_m g, \tag{4a}$$

$$0 = -\frac{\partial P}{\partial r} + \mu_m \frac{\partial^2 u}{\partial z^2}. \tag{4b}$$

Let $h(r,t)$ denote the foam height. Integrating (4a) from depths z and h, we find:

$$0 = P(r,z,t) - P(r,h,t) + \rho_m g(h-z). \tag{5a}$$

Outside the foam, the pressure distribution is hydrostatic in a liquid considered to be pure working fluid because the amount of bubbles present is very small (less than 2% in volume). Thus:

$$P(r,\, h,\, t) = P_{l0} + \rho_l g h, \tag{5b}$$

where P_{l0} is the pressure in the bulk liquid at depth $z = 0$ (at the conduit entrance). Combining (5a) and (5b) yields:

$$P(r,\, z,\, t) = P_{l0} + (\rho_l - \rho_m) g h + \rho_m g z. \tag{6}$$

Using (2b), this simplifies to:

$$P(r,\, z,\, t) = P_{l0} + \epsilon \rho_l g h + \rho_m g z. \tag{7}$$

The pressure at the top of the foam, which will be of interest in the next section, is therefore:

$$P(r,\,0,\,t) = P_{l0} + \epsilon\rho_l g h. \tag{8}$$

Using (7), equation (4*b*) yields:

$$\mu_m \frac{\partial^2 u}{\partial z^2} = \epsilon\rho_l g \frac{\partial h}{\partial r}. \tag{9}$$

This equation can be integrated with the following boundary conditions:

$$u(r,0,t) = 0, \tag{10a}$$

$$\frac{\partial u}{\partial z}(r,h,t) = 0. \tag{10b}$$

Condition (10*a*) states that there is no slip along the roof, for reasons given in Appendix A. Condition (10*b*) states that the shear stress vanishes at the bottom of the foam, along the interface with the bulk liquid. This is not strictly exact, since the flowing foam induces flow in the adjacent liquid, but represents a reasonable approximation in a deep tank such as the one used here (see the discussion in Huppert 1982). Using those, one finds:

$$u(r,z,t) = \frac{\epsilon\rho_l g}{2\mu_m}\frac{\partial h}{\partial r} z(z-2h). \tag{11}$$

Finally, we use the continuity equation which states that the foam volume contained between cylinders of radii (r) and ($r+\mathrm{d}r$) varies according to the horizontal fluxes across the sides of the cylinders and the vertical flux due to the bubbles from below. If the total gas flux is Q, then the corresponding flux of foam is Q/ϵ, and the vertical flux per unit area q is:

$$q = \frac{Q}{\epsilon S}, \tag{12}$$

where S is the cross-section of the tank. The horizontal foam flux across the side of a cylinder of radius r is:

$$\phi(r,t) = 2\pi r \int_0^h u\,\mathrm{d}z. \tag{13a}$$

The continuity equation is:

$$2\pi r \frac{\partial h}{\partial t} = 2\pi r q - \frac{\partial \phi}{\partial r}. \tag{13b}$$

Substituting (11) into (13*a*) and then into (13*b*) yields the following equation for the foam height:

$$\frac{\partial h}{\partial t} = \frac{\epsilon\rho_l g}{3\mu_m}\frac{1}{r}\frac{\partial}{\partial r}\left(rh^3\frac{\partial h}{\partial r}\right) + q. \tag{14}$$

This equation can be made dimensionless using the following scales:

$$r = r_t r', \tag{15a}$$

$$h = \left\{\frac{3\mu_m Q}{\pi\epsilon^2\rho_l g}\right\}^{\frac{1}{4}} h', \tag{15b}$$

$$t = \left\{\frac{3\pi^3\mu_m\epsilon^2}{\rho_l g Q^3}\right\}^{\frac{1}{4}} r_t^2 t', \tag{15c}$$

where r_t is the tank radius. Throughout the following, dimensionless variables will be used and the primes dropped. Boundary conditions can be specified at the tank periphery and the conduit entrance. At the tank periphery, there is no influx of bubbles into the foam layer, hence:

$$\phi(1,t) = 0. \tag{16a}$$

At the conduit entrance, we take a 'wide' conduit condition, such that the rate of upward flow of bubbles is not limited by the conduit size. Hence, there is no limitation on the flux out of the foam layer. We assume that flow is such that it thins the foam to zero thickness:

$$h(r_c,t) = 0, \tag{16b}$$

where r_c is the conduit radius. In principle, we should solve for the foam thickness at the conduit edge. However, the lubrication equations are no longer valid there and it has been shown that the simplified boundary condition (16*b*) does not lead to significant differences (Singh & Birkebak 1969; Beckett & Poots 1975).

Together with the obvious initial condition $h(r,0) = 0$, the problem is completely specified. We found no analytical solution to (14*b*) and we integrated it numerically. Figure 7 shows the solution at various times for $r_c = 0.157$. The behaviour of the foam layer can be described simply as follows. For small times and away from the conduit, the foam thickness is constant and increases linearly with time as $h = t$ (figure 8). Close to the conduit, flow into the conduit acts to thin the foam. This effect develops with time, affecting increasingly larger portions of the foam, and can be seen as a 'front' moving radially outwards. The behaviour can be understood better by a similarity solution developed for the two-dimensional equivalent of (14*b*) in Appendix B.

For large times, the foam adopts a steady-state geometry, whereby flow into the conduit balances exactly the input of bubbles from below. The steady-state equation for the foam thickness is:

$$\frac{1}{r}\frac{\mathrm{d}}{\mathrm{d}r}\left(rh^3\frac{\mathrm{d}h}{\mathrm{d}r}\right) = -1, \tag{17}$$

which, together with boundary conditions (16*a*, *b*) yields:

$$h_s(r) = \{2\ln(r) - r^2 - 2\ln(r_c) + r_c^2\}^{\frac{1}{4}}. \tag{18}$$

This describes the steady foam flow found with the silicone oil of lowest viscosity (10^{-2} Pa s).

An important feature of the solution in figure 7 is that, for any given gas flux, the foam thickness never exceeds a maximum value which is its steady-state value at the tank periphery:

$$h_m = \{-2\ln(r_c) + r_c^2 - 1\}^{\frac{1}{4}}. \tag{19}$$

The other important feature of this solution is given by the scaling relationship in (15*b*), i.e. the foam thickness increases with both the gas flux Q and the liquid viscosity μ_l.

This solution describes the experiments when there is no coalescence. To understand the process of coalescence, we turn to the internal structure of the foam and ask whether it is dynamically stable.

3.2. *The behaviour of bubbles within the foam layer*

The essential phenomenon is the deformation of bubbles by buoyancy forces as they tend towards close packing conditions in the foam layer. Consider first the well-known case of an isolated bubble stuck against the horizontal tank roof (e.g. Lee &

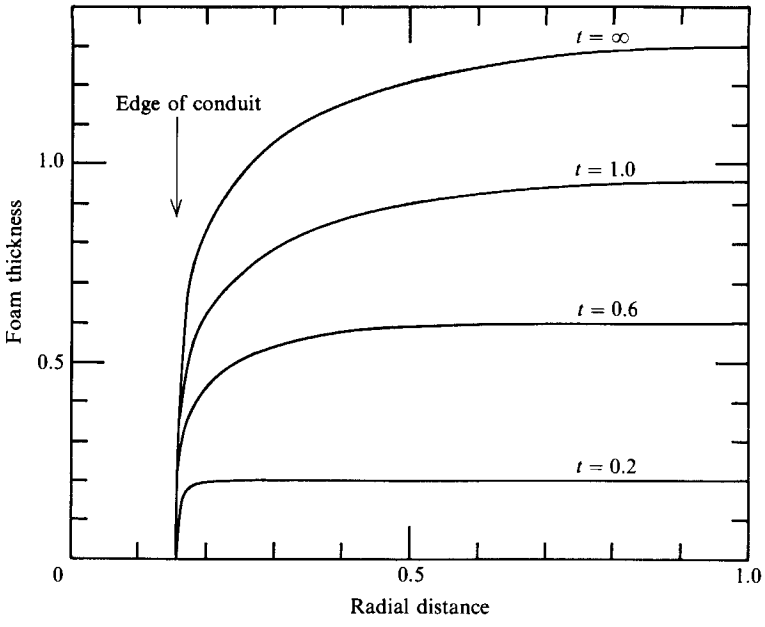

FIGURE 7. Foam thickness as a function of radial distance for three different times and at steady-state, in non-dimensional variables.

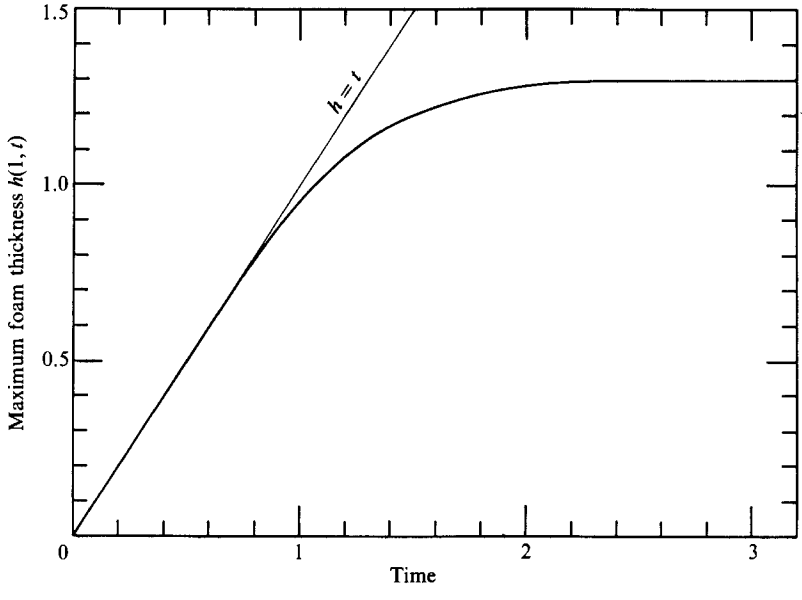

FIGURE 8. Foam thickness at the tank periphery $h(1, t)$ as a function of time in non-dimensional variables. Note that, for small times, the thickness increases as t.

Hodgson 1968): buoyancy acts to flatten it and leads to an approximately flat and circular contact area of radius b (figure 9). Equilibrium of the bubble is achieved through a balance between its buoyancy and excess pressure ΔP in the liquid film above it (the pressure exerted by the roof):

$$V(\rho_l - \rho_g)\, g = \Delta P \pi b^2, \tag{20a}$$

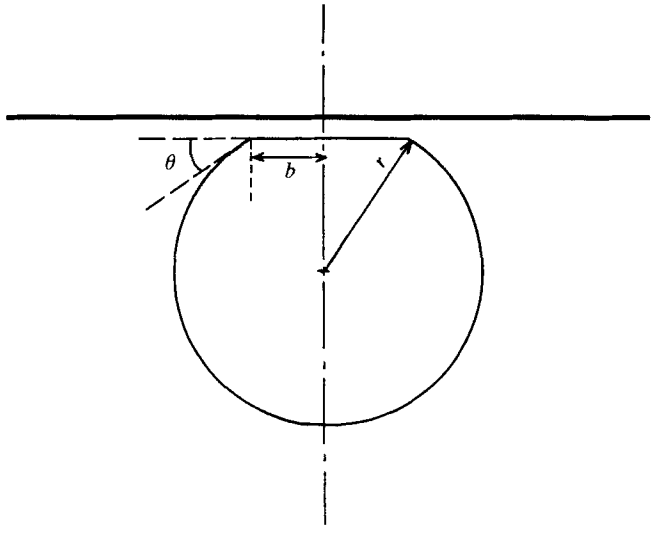

FIGURE 9. Schematic representation of a single bubble flattening against a rigid horizontal surface under its own buoyancy. b is the radius of the circular contact area and r the radius of curvature of the bubble walls just below this contact area. The finite contact angle θ is only a convenient geometrical simplification. The liquid film above the bubble is thick enough so that molecular effects are negligible and hence there is no 'dispersive pressure' in the film (e.g. Princen 1979). Thus, in reality, there is no discontinuity in the curvature of the bubble walls.

where V is the bubble volume. Across the flat film, pressure is continuous, and gas inside the bubble is also with excess pressure ΔP. Just below the edges of the flat film, this excess pressure is balanced by surface tension of the curves gas/liquid interface and hence:

$$\Delta P = \frac{2\sigma}{r}, \tag{20b}$$

where σ is the coefficient of surface tension and r the radius of curvature of the bubble close to the flat contact area (see figure 9). In this problem, pressure variations are small and we neglect the compressibility of the gas phase. Thus, V is equal to the original bubble volume of $\frac{4}{3}\pi R^3$. If bubble deformation is not large, i.e. if buoyancy is not large, r is close to the original radius R and we obtain the following expression for b:

$$b = R^2\left(\frac{2}{3}\frac{(\rho_1-\rho_g)\,g}{\sigma}\right)^{\frac{1}{2}}. \tag{21}$$

The important fact is that b decreases with increasing σ, which reflects the role of surface tension in resisting deformation.

In our experiments, the bubbles are in a foam and hence take more complex shapes. We again focus on the bubbles at the tank roof, which must support the buoyancy of the whole foam. Consider first moderate packing conditions corresponding to moderate foam heights (the qualification 'moderate' will be defined below). Under those conditions, the contact area is circular by symmetry with radius b. For a foam volume V_m with horizontal area S_m, the total buoyancy force F is acting on n bubbles at the roof. Each bubble thus supports a force F/n, and the same argument as before leads to:

$$(1/n)\,V_m\,g(\rho_1-\rho_g)\,e = 2\pi\sigma(b^2/r). \tag{22}$$

Now, each bubble at the roof occupies a cross-sectional area S' in the horizontal plane, and, by definition, neglecting the small area occupied by the liquid films between neighbouring bubbles:

$$nS' = S_m. \tag{23}$$

Using $V_m = hS_m$ and neglecting the gas density, we find:

$$S' h_g \rho_l \epsilon = 2\pi\sigma(b^2/r), \tag{24a}$$

which can be rewritten as:

$$h = \frac{2\sigma}{\epsilon\rho_l g}\frac{1}{r}\left(\frac{\pi b^2}{S'}\right). \tag{24b}$$

If the radius of curvature does not vary much, this equation has the simple interpretation that, as h increases, the bubble flattens such that the ratio of contact area to cross-section increases. Maximum flattening is thus such that this ratio reaches the value of 1.

To proceed further, one needs to specify the geometrical characteristics of packing. As shown by several studies, the probable packing configuration is a sphere truncated by a rhomboidal dodecahedron (RDH packing, see Princen, Aronson & Moser 1980) (figure 10). The radius of curvature, r, of the deformed bubble edges, is thus equal to the radius of the truncated sphere. Each face is a rhombus located at a distance $\frac{1}{2}a$ from the RDH centre, with long diagonal a and small diagonal $a/\sqrt{2}$. A cross-section through the RDH along four long diagonals of length a (figure 11) yields:

$$\cos\theta = \tfrac{1}{2}a/r. \tag{25}$$

The volume of the deformed bubble can be calculated as:

$$V = \frac{\pi a^3}{6}\left[-\frac{5}{\cos^3\theta}+\frac{9}{\cos^2\theta}-3\right]. \tag{26a}$$

Or, using (25):

$$V = \tfrac{4}{3}\pi r^3(-5+9\cos\theta-3\cos^3\theta). \tag{26b}$$

If the foam thickness is not large, pressure variations are small and compressibility effects are negligible. If R denotes the original bubble radius, volume conservation for each bubble yields:

$$r/R = (-5+9\cos\theta-3\cos^3\theta)^{-\frac{1}{3}}. \tag{27}$$

Numerical calculation shows that the ratio r/R remains close to 1. This can be seen by the Taylor series expansion of (27):

$$r/R = 1+\tfrac{3}{4}\theta^4+O(\theta^8). \tag{28}$$

Thus the radius of curvature of the bubble edges remains very close to the original radius. The packing geometry also yields the cross-section S' of the deformed bubble (figure 11) and we find, using (24b):

$$h = \left(\frac{2\sigma}{\epsilon\rho_l g}\right)\frac{1}{r}\frac{\pi}{3\sqrt{2}}tg^2\theta. \tag{29a}$$

Because r remains equal to R for all practical purposes, this equation shows how the contact angle at the roof increases as a function of the foam thickness. The equation is valid only when h is larger than the bubble diameter and hence does not apply for very small values of θ.

The RDH packing configuration is only an approximation. However, other

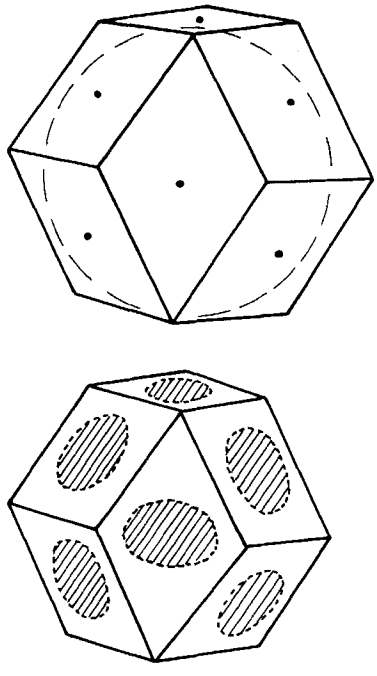

FIGURE 10. Geometrical configuration for bubbles in RDH packing. Each bubble is inscribed in a rhomboidal dodecahedron and develops flat contact areas with each face.

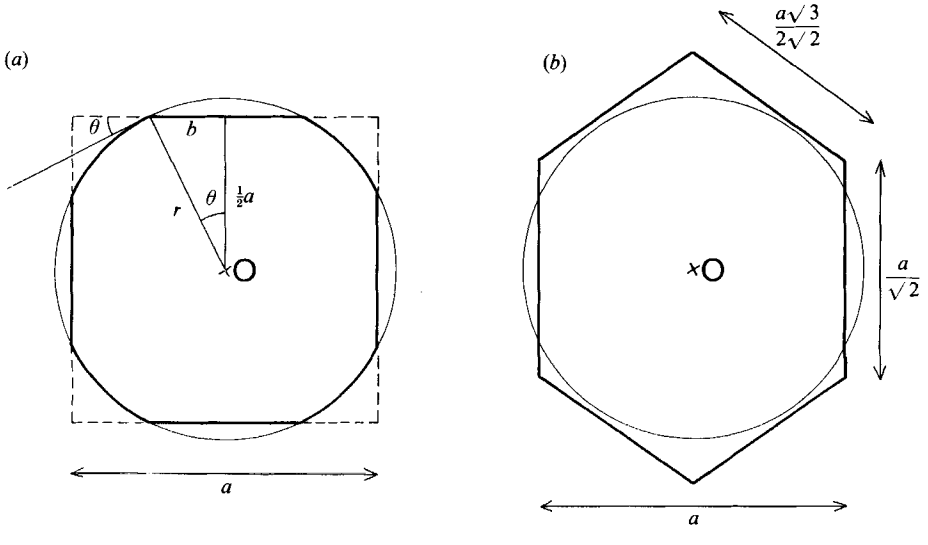

FIGURE 11. Two cross-sections through a bubble in RDH packing. (*a*) Through the four long diagonals, i.e. in a plane perpendicular to the contact area. (*b*) Through the median horizontal plane of the dodecahedron.

configurations would only lead to different coefficients in (27) and (29*a*). For example, (29*a*) takes the general form:

$$h = \left(\frac{2\sigma}{\epsilon\rho_1 g}\right)\frac{1}{R}f(\theta), \tag{29b}$$

where $f(\theta)$ is some increasing function of contact angle θ. The RDH geometry cannot be used for contact angles greater than 30°. This limit-angle is such that the circular contact areas become tangent to the edges of the rhombi (figure 10). For larger values of the contact angle, there is no generally accepted geometry. The system must tend towards a polyhedral foam and some modification of the figure of a regular pentagonal dodecahedron is usually considered (Princen *et al.* 1980). It is not possible to specify simply how packing develops under those conditions. By continuity, we assume that the radius of curvature of the film edges remains close to R, the original bubble radius. The maximum packing condition is such that the contact area becomes equal to the cross-sectional area of the bubble (see above). Using (24*b*), the maximum foam height is thus:

$$h_c = \frac{2\sigma}{\epsilon\rho_1 g}\frac{1}{r} \approx \frac{2\sigma}{\epsilon\rho_1 g}\frac{1}{R}. \tag{30}$$

Although this does not constitute a rigorous proof, we shall provide experimental verification for this relationship.

3.3. *The phenomenon of foam collapse*

To summarize the preceding argument, there is a critical thickness above which bubble deformation becomes insufficient to balance buoyancy. If the foam is thinner than this value, it is stable and steady form flow occurs. If its thickness reaches the critical value, it is no longer stable and we assume that this defines the condition for collapse. The critical thickness depends neither on the fluid viscosity nor on the gas flux. As shown by the scaling relationship (15*b*), increasing the foam thickness to the critical value can be achieved by increasing either the liquid viscosity or the gas flux. This explains our experimental findings. A final verification is provided by the experiment with the 85% glycerol solution. This liquid has almost the same viscosity as the 0.1 Pa s silicone oil which exhibits marked foam collapse for gas fluxes above 100 cm^3/min (figure 5*c*), yet requires a gas flux in excess of about 1400 cm^3/min to produce the same effect. This is because surface tension is higher (table 1), which implies a higher critical thickness and hence a higher critical gas flux.

The criterion for foam collapse is thus:

$$h_m = h_c. \tag{31}$$

The critical gas flux Q_c is thus such that the maximum foam thickness at that gas flux is equal to h_c:

$$A\left(\frac{3Q_c\mu_m}{\pi\epsilon^2\rho_1 g}\right)^{\frac{1}{4}} = \frac{2\sigma}{\epsilon\rho_1 gR}, \tag{32a}$$

where A is the constant deduced from (15*b*) and (19):

$$A = \left(-2\ln\left(\frac{r_c}{r_t}\right)+\frac{r_c^2}{r_t^2}-1\right)^{\frac{1}{4}}. \tag{32b}$$

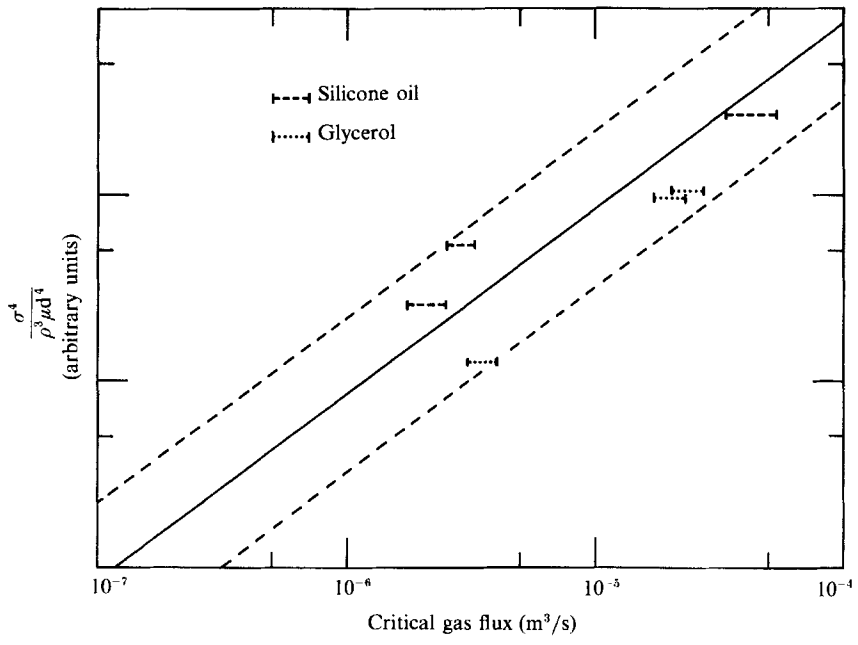

FIGURE 12. Plot of the critical gas flux for foam collapse as a function of parameter group $\sigma^4/\rho_l^3 \mu_l d^4$ (equation (33*b*)). The thick line and the two dashed lines correspond to three values of the gas volume fraction: the mean value of 0.69 and the two extreme values of 0.61 and 0.76 respectively.

Using (3) for the foam viscosity, we obtain:

$$Q_c = \frac{\pi}{3}\left\{\frac{4}{A}\right\}^4 \frac{1}{g^3} \frac{(1-\epsilon)^{\frac{5}{2}}}{\epsilon^2} \frac{\sigma^4}{\rho_l^3 \mu_l d^4}, \tag{33a}$$

where the bubble diameter d has been used instead of the radius R. If the gas volume fraction ϵ is constant, this can be expressed as:

$$Q_c = B \frac{\sigma^4}{\rho_l^3 \mu_l d^4}, \tag{33b}$$

where B is a coefficient which depends on the value of ϵ. Thus, the critical gas flux should be proportional to the parameter group $\sigma^4/\rho_l^3 \mu_l d^4$.

The critical gas flux has been determined for our different fluids. This was done using the gas volume data and determining the gas flux for which the curves for the minimum and maximum gas volumes intersect each other. These estimates are plotted against the parameter group defined in (33*b*) in figure 12. The theory predicts that the data points should lie on a line of slope 1, which is indeed approximately true. There is some scatter, which we attribute to small changes in the gas volume fraction ϵ. As shown by (33*a*), a small difference in the value of ϵ changes the value of the critical gas flux by a large amount: for ϵ increasing from 0.6 to 0.7, say, the critical gas flux decreases by a factor of 3. The coefficient of proportionality for the best-fitting line drawn through the data points in figure 12 is 1.2×10^{-2} and yields a value of 0.69 for ϵ. The two extreme lines which enclose all data points correspond to values of 0.61 and 0.76 for ϵ. These values are not absurd: packing with touching spheres is achieved at a volume fraction of 0.74 and departures from this value can

be expected when the liquid films between neighbouring bubbles have a non-negligible thickness. The simple theory thus yields reasonable numerical results, even though the equations are extremely sensitive to the value of ϵ. For example, selecting a value of 0.5 for ϵ, outside the range of what can be called a foam, the coefficient of proportionality in (33*b*) would be 1.6×10^{-1}, well outside the observed range of 0.5×10^{-2}–2.7×10^{-2}.

We emphasize that this range of gas volume fractions is within the range of the data by Sibree (1934) on the viscosity of foams. These data were used to establish (3) for the foam viscosity (Appendix A), and hence the implied viscosity values are not an artefact of this equation.

3.4. *A limit case: instantaneous foam collapse*

At values of the gas flux above the critical value, foam collapse occurs. This is achieved through bubble bursting, which is a poorly understood phenomenon (Bikerman 1973). We assume that bursting and foam collapse are instantaneous. The critical gas flux is such that the foam reaches just the critical thickness at steady-state. For a higher gas flux, the foam reaches the critical thickness at a smaller time, when it has not yet adopted its steady-state shape. In those conditions, the foam is flat away from the conduit (figure 7). When it breaks down, its thickness is equal to the critical value over an annulus confined between the tank periphery and some intermediate radius, and collapse should affect all this region. This is indeed true, as shown by a close-up of the tank roof (figure 13). As the gas flux increases further, collapse occurs earlier when the flat portion of the foam is larger. This implies that the gas pocket volume increases, and explains the data presented in figure 5(*b*, *c*).

The theory is not adequate to make accurate predictions of the gas pocket volume. From the mathematical point of view, the foam thickness has a strict maximum at the tank periphery ($r = r_t$), and is smaller than this everywhere. Thus, the criterion $h = h_c$ taken strictly leads to a gas pocket of vanishing volume. In reality, in analogy with nucleation phenomena in undercooled melts, the foam thickness must exceed the critical value by some small but unspecified amount. A small variation in the criterion for instability leads to variations in the area affected by collapse and hence in the gas pocket volume. Given this difficulty, the regularity of the experiments is remarkable. The theory does, however, allow an approximate check on the value of the erupted volume. Clearly, the maximum volume corresponds to a foam with thickness h_c everywhere and is therefore given by:

$$V_p = \epsilon\pi(r_t^2 - r_c^2)\, h_c. \tag{34}$$

This volume can be obtained at high values of the gas flux, when the foam reaches the critical thickness before flow into the conduit has time to develop. For the mean volume fraction of 0.69 and the bubble diameter appropriate for large values of the gas flux (table 2), the critical thickness is about 5.4 mm, which is compatible with direct visual observation. Equation (34) implies that the maximum foam volume is about 330 cm^3 and the corresponding gas volume about 230 cm^3. At high values of the gas flux in excess of about 1600 cm^3/min, the erupted volume depends little on the gas flux for both the 0.05 and 0.1 Pa s silicone oils, taking approximately constant values of 200 ± 40 cm^3 and 230 ± 40 cm^3 respectively (figure 5*b*, *c*). These are consistent with the previous estimate.

A better check of the model is provided by measurements of the intermittency, i.e. the time between two events of foam collapse. At high gas flux (sufficiently above the critical value), the foam reaches the critical thickness in a short time, before being

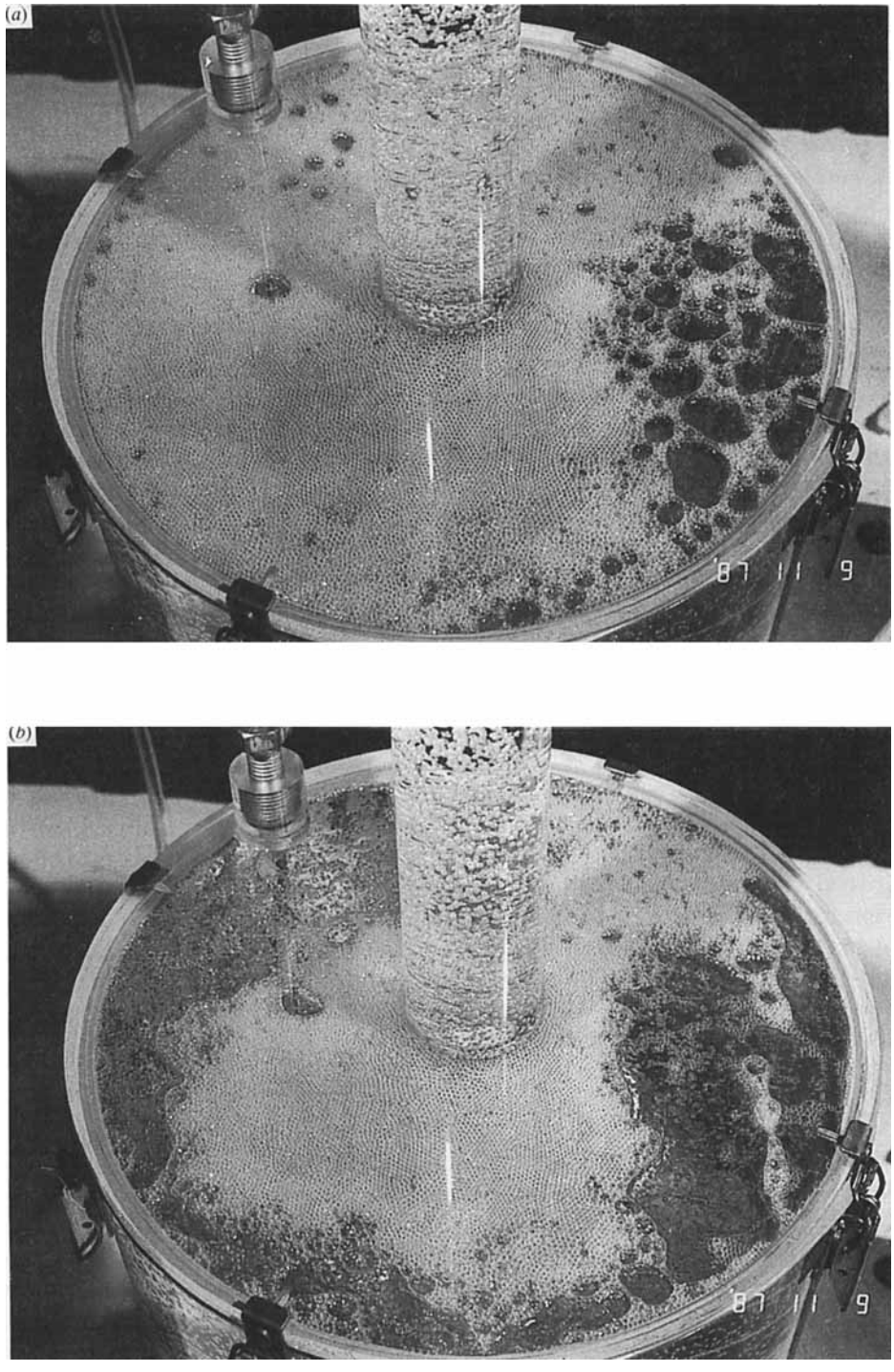

FIGURE 13. Close-up of the tank roof when foam collapse occurs (for 0.1 Pa s silicone oil). Note that the bubbles burst and coalesce in an annulus close to the tank periphery.

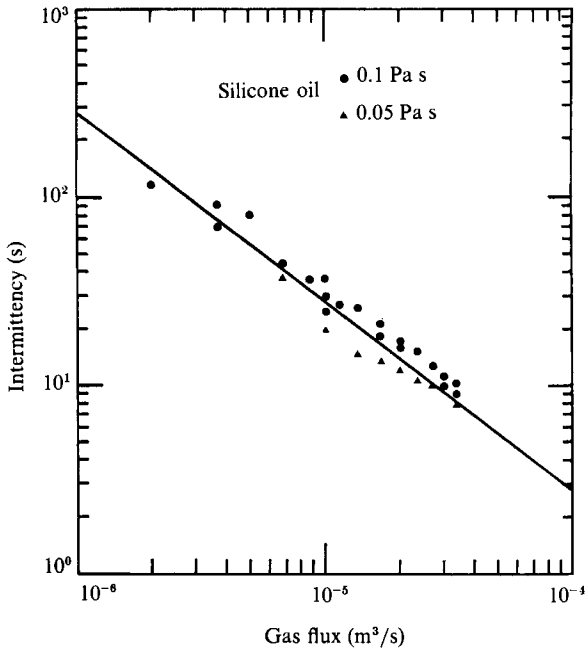

FIGURE 14. Intermittency (i.e. the time between two events of foam collapse) as a function of gas flux. The thick line is theoretical relationship (36) for a mean bubble diameter of 2 mm.

affected by flow into the conduit over a large area. Away from the conduit, its thickness grows proportional to time and to the flux per unit area q (figure 8). Thus, the time t_c needed to reach the critical thickness h_c is given by:

$$qt_c = h_c. \tag{35}$$

Using (12) for q as a function of the overall gas flux Q and (30) for the critical thickness, we find:

$$t_c = \pi r_t^2 \frac{4\sigma}{\rho_l g d} \frac{1}{Q}. \tag{36}$$

The interest of this relationship is that it depends neither on the gas volume fraction ϵ which is not determined directly, nor on the foam viscosity which is not known accurately. If the bubble diameter d does not vary much, it predicts that the intermittency is inversely proportional to the gas flux. The relationship is plotted in figure 14 and compared to data for two different silicone oils for a mean bubble diameter of 2 mm appropriate for those cases (table 2). The agreement is good.

3.5. *Non-instantaneous foam collapse*

We have so far assumed that the foam collapses instantaneously into a single gas pocket when the critical thickness is reached. This provides a good description of the experiments made with the silicone oils up to a viscosity of about 0.1 Pa s. For the more viscous oils, we observed a different regime in which pockets of intermediate size are generated and flow intermittently into the conduit (figure 4). For those liquids, the foam does collapse, but the process is sluggish. We observed that bubbles burst to form a gas pocket which slowly grows while being transported in the foam. The gas pocket erupts when it reaches the conduit edge but, at that point, the whole foam has not collapsed and there are many similar pockets being carried towards the

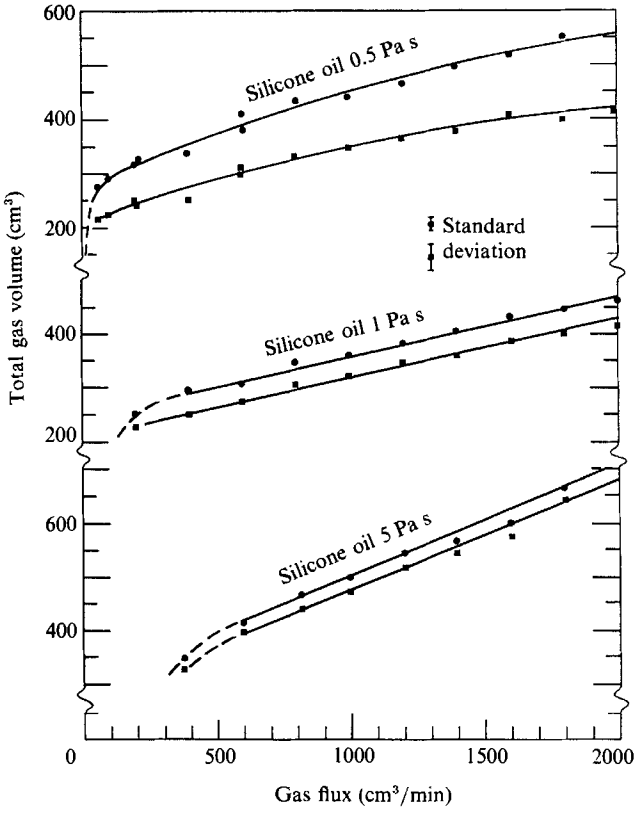

FIGURE 15. Total gas volume as a function of gas flux for the intermittent slugging regime, shown for three silicone oils of increasing viscosity. Note that the volume of the gas pockets decreases as viscosity increases.

conduit. We interpret this as being due to the phenomenon of bubble bursting, which is of a probabilistic nature. When the foam reaches the critical thickness, collapse starts at a certain number of 'nucleation' sites. In the low viscosity oils, we observed that collapse propagates across the foam very rapidly (figure 3) and results in a single gas pocket. At higher viscosity, each 'nucleation' site generates an individual pocket which grows slowly. Growth becomes slower as liquid viscosity increases, leading to smaller gas pockets (figure 15). We have no theory for this regime and develop a qualitative argument.

We focus on the individual bursting phenomenon. Consider two touching bubbles. By Laplace's law, the gas inside each bubble is at pressure P_i above the ambient pressure P:

$$P_i - P = 2\sigma/R. \tag{37}$$

When they burst, these two bubbles coalesce into a single gas pocket. Assuming isothermal conditions, the pressure inside the gas pocket is initially at the same pressure P_i, which is not in equilibrium with surface tension along the now larger boundary. Gas must expand to re-establish equilibrium. This promotes the bursting of the bubbles which surround the pocket, which thus enlarges by successive additions. In a viscous liquid, as the pocket grows larger, its expansion is limited by viscous forces along its outer boundary. If the pocket is large compared to the bubble size, the lengthscale of the deformation is large and it may be considered that the

	Viscous growth τ_g	Residence in foam layer τ_r	Drainage τ_d
Silicone oils			
47V10	0.02	8	7
47V50	0.11	12	15
47V100	0.25	14	18
47V500	2.0	21	28
47V1000	4.5	25	32
47V5000	35.0	37	41
Glycerols			
85%	0.13	15	48
89%	0.19	16	51
99%	1.8	25	75

TABLE 3. Characteristic times of various phenomena (in seconds, for a nominal gas flux of 2000 cm^3/min)

surrounding medium which is being deformed is the foam of effective viscosity μ_m. Assuming spherical geometry for simplicity, and neglecting inertial terms, the governing equation for the gas pocket is (Rosner & Epstein 1972):

$$4\mu_m \frac{\dot{R}_p}{R_p} = P_i - P - \frac{2\sigma}{R_p}, \tag{38}$$

where R_p is the pocket radius. If the pocket is large compared to the initial bubble size, then the capillary pressure term in this equation can be neglected. Because the pocket does not need to expand much to promote the bursting of neighbouring bubbles, the driving pressure difference stays close to the initial value given by (37). Thus:

$$4\mu_m \frac{\dot{R}_p}{R_p} \approx \frac{2\sigma}{R}. \tag{39}$$

From this, the viscous timescale for the pocket growth is:

$$\tau_g = \mu_m d/\sigma. \tag{40}$$

The time available for growth is simply the residence time in the foam, whose characteristic value is given by the scaling relationship in (15*c*):

$$\tau_r = \left(\frac{3\pi^3 \mu_m \epsilon^2}{\rho_l g Q^3}\right)^{\frac{1}{4}} r_t^2. \tag{41}$$

The ratio τ_g/τ_r gives a rough estimate of the number of coalescence events which enlarge the gas pocket as it is transported towards the conduit, and hence allows an estimate of the pocket volume which will be erupted. Table 3 compares the two characteristic times. The growth time is proportional to μ_l and the residence time to $\mu_l^{\frac{1}{4}}$. The ratio τ_g/τ_r therefore increases with liquid viscosity. Roughly speaking, in the experiment with 0.05 Pa s silicone oil, about one hundred coalescence events are possible during flow to the conduit, whereas less than ten such events are possible for 5 Pa s oil. This accounts for the regular decrease in erupted volume as a function of liquid viscosity (figure 15).

4. Discussion

4.1. *Drainage of liquid*

We have treated the foam as having a constant and uniform gas fraction ϵ. In reality, bubbles always rise with respect to the liquid and liquid drains out of the foam. Therefore the gas volume fraction must vary both in time and space. This process has been studied extensively, and depends strongly on the physical properties of liquid and gas (Bikerman 1973, pp. 159–183). Drew & Segel (1971) have shown that the general scaling law for the drainage time is:

$$\tau_d = \frac{k_1 h}{\epsilon(1-\epsilon)\rho_l g}, \tag{42}$$

where k_1 is some coefficient which depends on the geometry of the liquid regions, the gas volume fraction and liquid viscosity. By analogy with permeability laws, this can be written as

$$\tau_d = \frac{k_2 \mu_l h}{\epsilon(1-\epsilon)\rho_l g d^2}, \tag{43a}$$

where k_2 now depends only on the gas volume fraction and the packing configuration. In the limit of high ϵ, this expression can be simplified to:

$$\tau_d = \frac{k_2 \mu_l h}{(1-\epsilon)\rho_l g d^2}. \tag{43b}$$

A series of experiments at volume fractions exceeding 0.98 by Rand & Kraynick (1983) shows the validity of this relationship. These authors find that the time needed to drain half of the liquid initially present in a foam layer is:

$$\tau_d = \frac{580\,\mu_l h}{(1-\epsilon)\rho_l g d^2}. \tag{44}$$

Thus k_2 is independent of ϵ in the high volume fraction limit. In the absence of other data, we simply extend this law to smaller volume fractions to obtain a characteristic time for liquid drainage:

$$\tau_d = \frac{580\,\mu_l h}{\epsilon(1-\epsilon)\rho_l g d^2}. \tag{45}$$

The drainage time is similar to the residence time (table 3). At high gas flux, the residence time is not a proper measure of the time available for drainage because the foam collapses before reaching its steady-state shape. At 2000 cm^3/min, the foam exists for less than ten seconds (figure 14), which is a fraction of the drainage time and implies that only small amounts of liquid can drain out of it. The important fact is that the phenomena observed do not depend on the time available for drainage, as shown by the variation of intermitency with gas flux (equation (36) and figure 14). We conclude that drainage plays no important role.

4.2. *The physics of coalescence*

The exact process of film rupture is not well known, but must involve van der Waal forces between the liquid molecules. These forces become important when the film thickness is small, and most work on this problem has focused on how and where a film thins the most (e.g. Jones & Wilson 1978). Over a foam layer of large horizontal dimensions with many bubbles, there must be a statistical distribution of film

geometry and thickness. Hence, we may assume that there are always two bubbles with thin films where rupture can occur. This explains the fact that collapse appears to 'nucleate' at some location. Once collapse has started, the limiting factor is not some local effect in the film, but viscous stresses at the edges of the growing pocket, as argued in §3.5.

The criterion for foam collapse relies on a mechanical stability argument. Foam collapse is often attributed to shear, which acts to stretch and thin the liquid films between bubbles and eventually leads to their rupture (Princen 1979; Princen *et al.* 1980). In our experiments, the foam layer is flowing horizontally and shear stresses are indeed applied to the bubble walls. However, we have shown that collapse occurs first at the tank periphery (figure 13), where, by definition, there is no shear as shown by (16*a*) and (13*b*). The region of highest shear, in the vicinity of the conduit edge, sees little collapse (figure 13).

4.3. *The interpretation of volcanic regimes*

For application to natural systems, it is important to characterize simply the different regimes. Two dimensionless numbers can be defined. One is the ratio of the two characteristic heights:

$$N_1 = \left\{\frac{3Q\mu_m}{\pi\epsilon^2\rho_1 g}\right\}^{\frac{1}{4}} \Big/ \frac{4\sigma}{\epsilon\rho_1 g d}. \tag{46}$$

When N_1 is less than 1, the foam thickness is smaller than the critical value and steady foam flow is observed. When N_1 exceeds 1, foam collapse occurs. The eruption regime will be either cyclic activity or intermittent slug flow, depending on the value of a second dimensionless number, defined as the ratio between the growth time and the residence time:

$$N_2 = \frac{\mu_m d}{\sigma} \Big/ r_t^2 \left(\frac{3\pi^3\mu_m\epsilon^2}{\rho_1 g Q^3}\right)^{\frac{1}{4}}. \tag{47}$$

For very small values of N_2, collapse can be considered as instantaneous and cyclic activity results. When N_2 becomes of order 10^{-1}, say, only a few coalescence events are possible, and the slugging regime prevails. This criterion is somewhat ambiguous. However, in practice, the field observations are sufficient to discriminate between the two regimes: there can be little doubt that Hawaiian activity corresponds to the cyclic one and Strombolian activity to the slugging one.

To fully characterize an eruption, one needs to determine the bubble size in the magma chamber, the gas flux (the degassing rate) and finally the size of the chamber roof. We now discuss briefly the orders of magnitude likely to obtain for these variables in Kilauea volcano. The gas bubbles nucleate and grow in a saturated melt. Their minimum diameter is a few micrometres, the critical size of a stable nucleus (Sparks 1978). The bubbles grow essentially by diffusion and, during the few weeks of an effusive episode, can reach a diameter of about 1 cm (Sparks 1978). For the surface tension of water vapour in basalt (0.4 kg s^{-2}, Williams & McBirney 1979), the critical foam thickness is therefore between 4 cm and 40 m. The area of the chamber roof must be larger than that of summit calderas (collapse features attributed to foundering of the chamber), which is about 10 km^2. Therefore, rough estimates for the gas pocket volume lie between 4×10^5 and 4×10^7 m^3. At the ambient pressure in the chamber which must be somewhat higher than 5×10^7 Pa if the top of the chamber is at a depth of about 2 km, the water density is at least 100 kg m^{-3}, and hence the mass of gas contained in the pocket may be between 4×10^7 and 4×10^9 kg. During an effusive episode, about 10^7 m^3 of melt of bulk density

2700 kg m^{-3} are produced in three weeks (Swanson *et al.* 1979). For the 0.5 wt% concentration suggested by Greenland (1987), the corresponding mass of water is about 10^8 kg, which lies within the previous range. This comparison is not meant to imply that these two gas contents must be equal, but to show that our model does not require a large mass of gas compared to that which is available. The wide range of values for the various parameters of interest is disappointing, but we show in a companion paper that a detailed analysis of Hawaiian eruptions allows strong constraints on them.

It is clear that the flat roof and simple geometry of our experimental tank may be far removed from the true structure of a volcano. This is an obvious difficulty and several points must be emphasized in this respect. The essential phenomenon is the breakdown of a foam layer when it reaches the critical thickness. In any situation, the foam thickness is determined by a balance between the input of bubbles from below and the output into the conduit. A complex roof geometry (sloping for example) affects the details of this balance but there is always a gas flux for which the foam thickness exceeds the critical value. The robust result of this paper is the equation for the critical foam thickness, which has been verified by two independent measurements: the critical gas flux and the intermittency. For any given roof geometry, it is possible to solve for the foam thickness as a function of gas flux, and hence to determine the condition for foam collapse. The problem is thus to specify the true roof geometry, which of course is not feasible. Volcanic eruptions are often more complex than the descriptions we have given, and it may be more appropriate to define a wide spectrum of regimes, with the 'Hawaiian' and 'Strombolian' definitions representing end-members. For example, Stromboli sometimes produces small fire fountains (Williams & McBirney 1979), and the 'gas piston' activity of Kilauean eruptions could well be called Strombolian. All these manifestations can be interpreted as the effect of gas pockets of various sizes and explained by irregularities of the chamber roof. If our hypothesis is valid, it is clear that only when the geometry is simple can the degassing process take a simple and repetitive form. Kilauea is probably close to our experimental conditions because it is a shield volcano with gentle slopes: there is room for a large magma chamber with an almost horizontal roof (see Ryan 1987).

We end the paper by a remark on the evolution of eruption conditions at Hawaii. We have stated that a Hawaiian eruption usually starts by a phase in which fire fountaining alternates with effusive activity or quiescence, and ends in the effusive regime only, without fire fountaining. The available data show that the output rate decreases throughout the eruption, which must be linked to a decrease of the degassing rate at depth. According to our model, when the degassing rate falls below the critical value, the cyclic regime with foam collapse becomes impossible, and this explains why fire fountaining stops.

5. Conclusion

The three possible regimes of degassing described in this paper reproduce many observed eruption characteristics of basaltic volcanoes. Fire fountaining may be due to the eruption of a large gas pocket, effusive activity to steady foam flow, and Strombolian intermittent explosive activity to the slugging regime. Thus, we suggest that all these volcanic manifestations are different forms of the same fundamental process: magma degassing in a large reservoir which empties into a narrow conduit.

As discussed in the introduction, there is strong evidence that degassing does occur

in the magma chamber of several well-known volcanoes. Therefore, unless the laboratory experiments violate a key feature of volcanic systems, the fluid dynamical phenomena we have documented must occur. The fact that phenomena closely resembling them do occur shows that, at least, this model of volcanic eruptions is self-consistent. Its interest lies in its ability to relate phenomena observed at the Earth's surface to processes occurring at depth.

We thank Stephen Tait, Donald Turcotte and Lionel Wilson for help and encouragement, and three anonymous referees for their useful remarks. This research was supported by a grant from INSU (CNRS, France). Contribution CNRS-INSU-DBT no. 47 (Thème Instabilités).

Appendix A. The rheological properties of foams

The rheological properties of foams have been studied extensively because of important industrial applications. However, there is no comprehensive theoretical or observational framework which allows their direct calculation as a function of liquid and gas physical properties, surface tension, and gas volume fraction (Kraynick 1988). Two cases are reasonably well understood: the dilute and 'dry' cases at small and high gas volume fractions respectively.

At small gas volume fractions, drop deformation gives rise to an elastic-like response (Schowalter 1978, pp. 271–275). Such effects are negligible at low shear rates and can be safely ignored in our experiments. The shear stress–strain rate relationship is unaffected by drop deformation and is linear (Schowalter 1978, p. 274), as in a Newtonian fluid, with viscosity given by:

$$\mu_{\mathrm{m}} = \mu_{\mathrm{l}}(1 + n\epsilon), \tag{A 1}$$

where n is a coefficient. For gas bubbles, n is usually taken to be 1 using the equation for dilute emulsions (Taylor 1932) and setting the gas viscosity to zero. However, dynamic interfacial phenomena contribute complex effects and, in general, n is greater than 1 (Kraynick, 1988, p. 330). The limiting case is when bubbles behave as rigid spheres and this corresponds to $n = \frac{5}{2}$.

At large gas volume fractions, bubbles are strongly deformed and separated by thin liquid films. Theoretical models are only available for two-dimensional foams (Khan & Armstrong 1986; Kraynick & Hansen 1987; Schwartz & Princen 1987). The latter one is the most realistic because it includes the effects of Plateau borders, which are the liquid regions lying at the intersection of three films. It predicts that foams are shear-thinning, with an effective viscosity which exceeds that of the liquid by a large amount, in agreement with experimental evidence. These foams also exhibit a yield stress, below which there is no flow, and the phenomenon of 'slip at the wall', where the thin liquid film which wets the bounding walls lubricates the flow (Princen 1985; Kraynick 1988).

We now discuss these important features of foam rheology in the context of our experiments. The foam layer which forms at the top of our tank has an intermediate gas volume fraction and is such that liquid continuously drains out as the bubbles are transported horizontally. The transition from quasi-Newtonian behaviour, which is a good approximation in the dilute case, to non-Newtonian behaviour must occur when the stretching of thin liquid films becomes an important phenomenon. This occurs at a gas volume fraction in excess of 0.74, the value for touching undeformed spheres where there are no such thin liquid films. For gas volume fractions less than

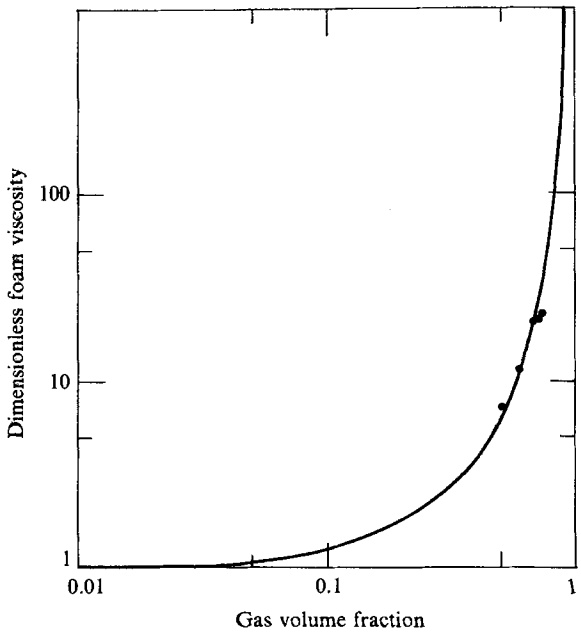

FIGURE 16. Dimensionless foam viscosity μ_m/μ_l as a function of gas volume fraction. The line corresponds to equation (A 5) and the dots are the original data from Sibree (1934).

this, we are aware of only one set of experiments by Sibree (1934). This author has often been quoted as saying that his foams exhibited shear-thinning behaviour. However, there is no such statement in his paper. This discrepancy can be attributed to the fact that he used a shear-thinning colloid as the continuous phase. In the shear rate domain where the viscosity of the continuous phase is constant, he found that the foams also have a constant viscosity. He interpreted his data in terms of the following relationship:

$$\frac{\mu_m}{\mu_l} = \frac{1}{1-(1.3\epsilon)^{\frac{1}{3}}}. \tag{A 2}$$

This relationship was an extension of an earlier one and allowed a reasonable fit to the data. It predicts that the foam viscosity becomes infinite at the finite volume fraction of 0.77. Foams are commonly prepared at much higher volume fractions and hence this equation is not adequate. It is simpler to look for a critical law of the form:

$$\frac{\mu_m}{\mu_l} = \frac{1}{(1-\epsilon/\epsilon_c)^n} \tag{A 3}$$

where ϵ_c is the critical volume fraction above which the foam breaks down, and n a critical exponent. There are foams with ϵ values in excess of 0.98 and a reasonable approximation is therefore $\epsilon_c \approx 1$. As ϵ goes to zero, (1.3) has the limiting form:

$$\frac{\mu_m}{\mu_l} = 1 + n\epsilon, \tag{A 4}$$

which can be compared to the expression for dilute foams (A 1). Depending on the behaviour of bubbles, the coefficient n can take values between 1 and $\frac{5}{2}$. Figure (16)

shows the data of Sibree (1934) plotted against the equation obtained with the latter value:

$$\frac{\mu_m}{\mu_l} = \frac{1}{(1-\epsilon)^{\frac{5}{2}}}. \tag{A 5}$$

The fit is excellent and hence we adopt (A 5) in our analysis. Interestingly, viscometric measurements using foams with gas contents between 0.88 and 0.99 show that, at low shear rates, shear stress is proportional to strain rate (Thondavadi & Lemlich 1985), with an effective viscosity similar to values predicted by this equation.

Yield stress is a strong function of liquid content and essentially drops to zero when the gas volume fraction decreases to a value of about 0.7 (Princen 1985). Furthermore, it is proportional to σ/R, whose value is very small in our experiments characterized by quite low surface tension and large bubbles (compared to most emulsions). We conclude that yield stress effects can be ignored in our case, or rather that they are not an adequate way to represent the behaviour of a loosely packed foam which is only a few bubbles in thickness.

Wall slip can be excluded on the same grounds. It is an important notion only at high gas volume fractions when there is a marked contrast between a foam with thin liquid films of small size and a continuous film of bulk liquid along the wall. Further, wall slip is found to decrease with shear stress (Princen 1985) and shear stresses are small in our experiments.

Appendix B. Similarity solution for two-dimensional foam flow

Consider now the two-dimensional case, in which a large rectangular tank is topped by a narrow slit through which liquid and foam can escape. This case is relevant to fissure eruptions on the flank of basaltic shield volcanoes. The two-dimensional equivalent of (14) is:

$$\frac{\partial h}{\partial t} - \frac{\epsilon \rho_l g}{3\mu_m} \frac{\partial}{\partial x}\left(h^3 \frac{\partial h}{\partial x}\right) = q, \tag{B 1}$$

where $h(x,t)$ is the foam thickness as a function of x, the distance away from the slit. The boundary and initial conditions are:

$$h(0,t) = 0, \tag{B 2a}$$

$$\lim_{x \to \infty} h(x,t) \text{ finite}, \tag{B 2b}$$

$$h(x,0) = 0. \tag{B 2c}$$

Equation (2.1) with conditions (2.2) has a similarity solution:

$$h(x,t) = qtH(\eta), \tag{B 3a}$$

where η is a similarity variable defined as follows:

$$\eta = \left(\frac{3\mu_m}{\epsilon \rho_l g q^3}\right)^{\frac{1}{2}} \frac{x}{t^2}. \tag{B 3b}$$

The equation for $H(\eta)$ is:

$$H - 2\eta \dot{H} + \frac{\mathrm{d}}{\mathrm{d}\eta}(H^3 \dot{H}) = 1, \tag{B 4}$$

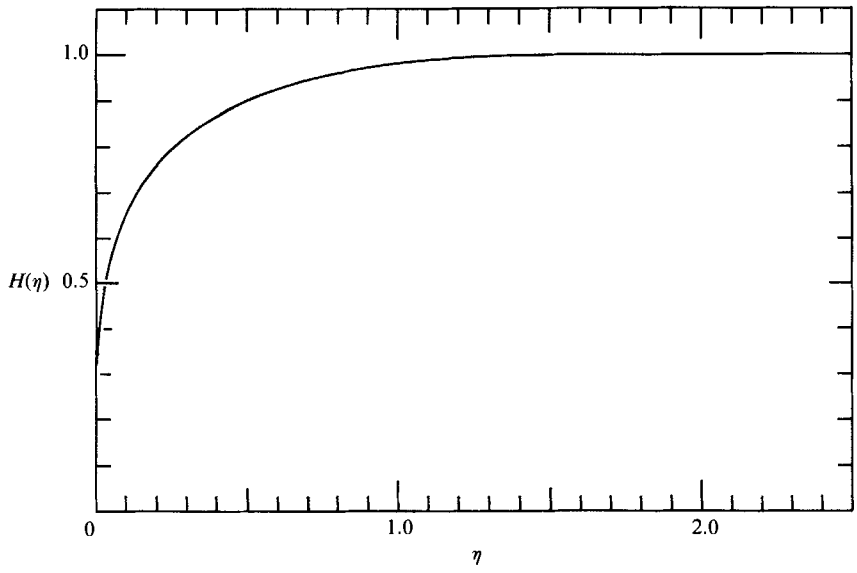

FIGURE 17. Similarity solution for a two-dimensional tank of infinite extent (from equation (B 4). The foam thickness is constant for values of η larger than about 1.5.

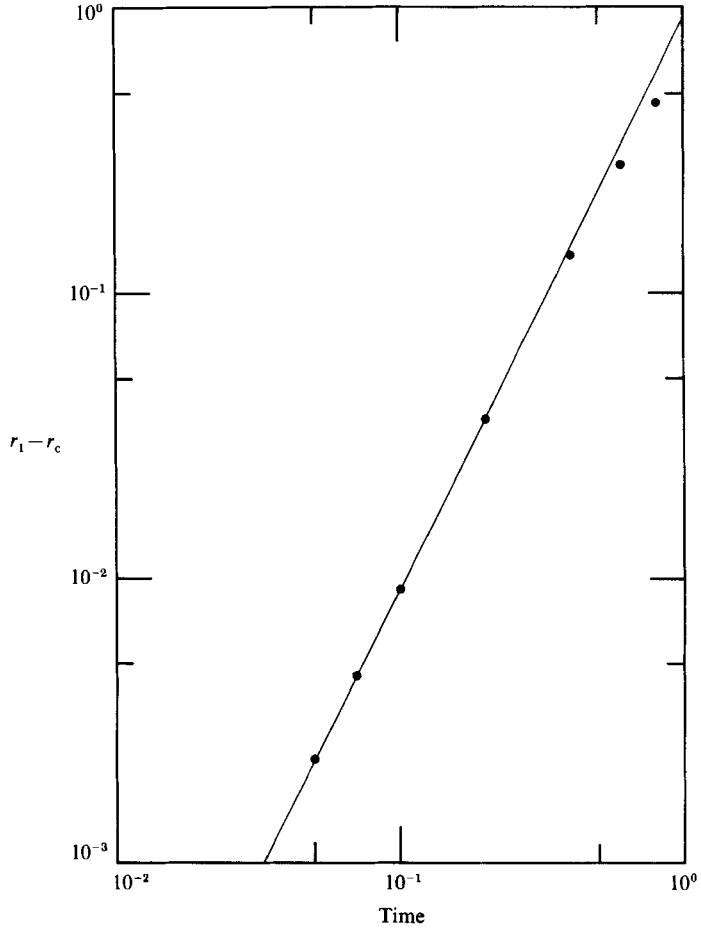

FIGURE 18. Plot of r_1-r_c (see equation (B 7) as a function of time for the cylindrical case studied in §3.3 (equation (14)): dots indicate results from the numerical integration of the equation and the line shows the similarity dependence $r(t) \propto t^2$ predicted by the analysis of Appendix B.

with the boundary conditions:

$$H(0) = 0, \tag{B 5a}$$

$$\lim_{\eta \to \infty} H(\eta) \text{ finite}. \tag{B 5b}$$

We found no analytical solution to (2.4) and have integrated the equation numerically (figure 17). The feature of this solution is that for η larger than about 1.5, the foam thickness is constant. In dimensional variables, this shows that, far from the conduit, the foam grows linearly with time because it is not affected by flow into the conduit. Flow into the conduit affects the foam for values of η between 0 and 1.5. In dimensional variables, this effect propagates as a 'front' located at x_n such that:

$$x_n = 1.5\left(\frac{\epsilon\rho_1 g q^3}{3\mu_m}\right)^{\frac{1}{2}} t^2. \tag{B 6}$$

In practice, the tank is of finite dimensions and this solution breaks down when the front reaches the tank edge.

In cylindrical coordinates, the boundary conditions are not compatible with such a similarity solution. It is not possible to specify both a finite foam height and a finite flux of foam with zero radius. The full numerical solution to (14) with finite conduit dimensions still exhibits the similarity behaviour at small times. Let r_1 be such that:

$$h(r_1, t) = (0.97)qt, \tag{B 7}$$

$(r_1 - r_c)$ varies approximately as t^2 for small times (figure 18), which is the functional dependence predicted by (B 6).

REFERENCES

BATCHELOR, G.K. 1967 *An Introduction to Fluid Dynamics*. Cambridge University Press. 615 pp.

BECKETT, P. M. & POOTS, G. 1975 Laminar film condensation on horizontal flat plates. *Mech. Res. Commun.* **2**, 61–66.

BIKERMAN, J. J. 1973 *Foams*. Springer. 337 pp.

BLACKBURN, E. A., WILSON, L. & SPARKS, R. S. J. 1976 Mechanisms and dynamics of Strombolian activity. *J. Geol. Soc. Lond.* **132**, 428–440.

CHOUET, B., HAMISEVICZ, N. & MCGETCHIN, T. R. 1974 Photoballistics of volcanic jet activity at Stromboli, Italy. *J. Geophys. Res.* **79**, 4961–4975.

CLIFT, R., GRACE, J. R. & WEBER, M. E. 1978 *Bubbles, Drops and Particles*. Academic Press. 380 pp.

DREW, D. A. & SEGEL, L. A. 1971 Analysis of fluidized beds and foams using averaged equations. *Stud. Appl. Math* **50**, 233–257.

GREENLAND, L. P. 1987 Composition of gases from the 1984 eruption of Mauna Loa. *US Geol. Surv. Prof. Pap.* 1350, 781–803.

HEAD, J. W. & WILSON, L. 1987 Lava fountains height at Pu'u'Oo, Kilauea, Hawaii: indicators of amounts and variations of exsolved magma volatiles. *J. Geophys. Res.* **92**, 13713–13719.

HUPPERT, H. E. 1982 The propagation of two-dimensional and axisymmetric viscous gravity currents over a rigid horizontal surface. *J. Fluid Mech.* **121**, 43–58.

JAUPART, C. & VERGNIOLLE, S. 1988 Laboratory models of Hawaiian and Strombolian eruptions. *Nature* **331**, 58–60.

JONES, A. F. & WILSON, S. D. R. 1978 The film drainage problem in droplet coalescence. *J. Fluid Mech.* **87**, 263–288.

KHAN, S. A. & ARMSTRONG, R. C. 1986 Rheology of foams: I: Theory for dry foams. *J. Non-Newtonian Fluid Mech.* **22**, 1–22.

KRAYNICK, A. M. 1988 Foam flows. *Ann. Rev. Fluid Mech.* **20**, 325–357.

KRAYNICK, A. M. & HANSEN, M. G. 1987 Foam rheology: a model for viscous phenomena. *J. Rheol.* **31**, 175–205.

LAMBERT, G., LECLOAREC, M. F., ARDOUIN, B. & LEROULLEY, J. C. 1985 Volcanic emission of radionuclides and magma dynamics. *Earth Planet. Sci. Lett.* **76**, 185–192.

LECLOAREC, M. F., PENNISI, M., ARDOUIN, B., LEROULLEY, J. C. & LAMBERT, G. 1988 Relationship between gases and volcanic activity at Mount Etna in 1986. *J. Geophys. Res.* **93**, 4477–4484.

LEE, J. C. & HODGSON, T. D. 1968 Film flow and coalescence: I: Basic relations, film shape and criteria for interface mobility. *Chem. Engng Sci.* **23**, 1375–1397.

PRINCEN, H. M. 1979 Highly concentrated emulsions, Part I. *J. Colloid Interface Sci.* **71**, 55–66.

PRINCEN, H. M. 1985 Rheology of foams and highly concentrated emulsions. II. Experimental study of the yield stress and wall effects for concentrated oil-in-water emulsions. *J. Colloid Interface Sci.* **105**, 150–171.

PRINCEN, H. M., ARONSON, M. P. & MOSER, J. C. 1980 Highly concentrated emulsions, Part II. *J. Colloid Interface Sci.* **75**, 246–270.

RAND, P. B. & KRAYNICK, A. M. 1983 Drainage of aqueous foams: generation pressure and cell-size effects. *J. Soc. Pet. Engng* **21**, 152–154.

ROSNER, D. R. & EPSTEIN, M. 1972 Effects of interface kinetics, capillarity and solution diffusion on bubble growth rates in highly supersaturated liquids. *Chem. Engng Sci.* **27**, 69–88.

RYAN, M. P. 1987 Elasticity and contractancy of Hawaiian olivine tholeiite and its role in the stability and evolution of subcaldera magma reservoirs and rift systems. *US Geol Surv. Prof. Pap.* 1350, 1395–1447.

SCHWARTZ, L. W. & PRINCEN, H. M. 1987 A theory of extensional viscosity for flowing foams and concentrated emulsions. *J. Colloid Interface Sci.* **118**, 201–211.

SCHOWALTER, W. R. 1978 *Mechanics of Non-Newtonian Fluids.* Pergamon. 300 pp.

SIBREE, J. O. 1934 The viscosity of froth. *Trans. Faraday Soc.* **30**, 325–331.

SINGH, S. N. & BIRKEBAK, R. C. 1969 Laminar free convection from a horizontal infinite strip facing downwards. *Z. angew. Math. Phys.* **20**, 454–461.

SPARKS, R. S. J. 1978 The dynamics of bubble formation and growth in magmas: a review and analysis. *J. Volcanol. Geotherm. Res.* **3**, 1–37.

SWANSON, D. A., DUFFIELD, W. A., JACKSON, D. B. & PETERSON, D. W. 1979 Chronological narrative of the 1969–71 Mauna-Ulu eruption of Kilauea volcano, Hawaii. *US Geol. Surv. Prof. Pap.* 1956. 59 pp.

TAIT, S. R., JAUPART, C. & VERGNIOLLE, S. 1989 Pressure, gas content and eruption periodicity of a shallow crystallising magma chamber. *Earth Plant. Sci. Lett.* in press.

TAYLOR, G. I. 1932 The viscosity of a fluid containing small drops of another fluid. *Proc. R. Soc. Lond.* A **138**, 41–48.

THONDAVADI, N. N. & LEMLICH, R. 1985 Flow properties of foam with and without solid particles. *Ind. Eng. Chem. Process Des. Dev.* **14**, 748–753.

THURBER, C. H. 1987 Seismic structure and tectonics of Kilauea volcano. *US Geol. Surv. Prof. Pap.* 1350, 919–934.

VERGNIOLLE, S. & JAUPART, C. 1986 Separated two-phase flow and basaltic eruptions. *J. Geophys. Res.* **91**, 12842–12860.

WILLIAMS, H. & MCBIRNEY, A. R. 1979 *Volcanology.* Freeman Cooper. 397 pp.

WILSON, L. 1980 Relationships between pressure, volatile content and ejecta velocity in three types of volcanic eruptions. *J. Volcanol. Geotherm. Res.* **8**, 297–313.

WILSON, L. & HEAD, J. W. 1981 Ascent and eruption of basaltic magma on the Earth and Moon. *J. Geophys. Res.* **86**, 2971–3001.